

# **Evaluation of transport properties in poly(3-hexylthiophene) using SCLC method and Controlled-Overflow-Transistor**

**Mohammad Fareed Ahmed**

Orientador

Prof. Dr. Ivo Alexandre Hümmelgen

Group of Organic Optoelectronic Devices,

Departamento de Física,

Universidade Federal do Paraná.

Curitiba-2013

“ Você acha ou você sabe?.....

It's so simple.....”

Professor Dr. I. A. Hümmelgen

# Abstract

---

Since the discovery of conducting polymers in 1977, a new era of research work has escalated, with applications such as transistors, solar cells, logic circuits, sensors, etc. The materials can be chemically modified during their synthesis in order to tailor the desired mechanical, electronic and optical properties of the final product. However, one of the main limitations of organic materials is due to the combination of its low mobility, presence of traps and unbalanced mobilities between positive and negative charge carriers. Several methods have been employed to determine the mobility such as time-of-light, field-effect transistor, etc.

The work presented in this thesis focuses on utilizing a simple method called Space-Charge-Limited current (SCLC) to determine the mobility of carriers in poly(3-hexylthiophene) (P3HT). P3HT is one of the most studied organic semiconductor polymer due to its high positive charge carrier mobility, good solubility and processability. Its positive charge carrier mobility has been evaluated by several methods including SCLC. However, the knowledge of its negative charge mobility is limited. In this work, we have investigated both the positive and negative charge carrier mobilities utilizing the SCLC method. Finally, the obtained values are compared to the obtained values by other methods that have already determined both of these mobilities.

Further, this work also sheds a new light on further enhancing the applications of low-mobility conducting polymers by using it in simple, cost effective hybrid transistor architecture. This transistor takes the advantage of the low mobility in conducting polymers and involves two regimes of operation at low and high electric field strengths. At low electric field, SCLC regime is formed and at high electric field strength thermionic regime is encountered. To our knowledge, this is one of a kind architecture. The device operation mainly depends upon the properties of the conducting polymer in use.

# Resumo Estendido

---

Os objetivos deste trabalho de tese são: (i) avaliar as propriedades de transporte do poly(3-hexylthiophene) (P3HT) utilizando o método de corrente limitada por carga espacial (SCLC); (ii) fabricar e caracterizar um transistor que denominamos Controlled-Overflow-Transistor (COT). Para isso, propomos um novo conceito de transistor, com base em SCLC e fenômenos emissão termiônica.

Esta tese está dividida em três seções: (1) Introdução e propriedades eletrônicas de semicondutores orgânicos, onde é apresentada uma visão geral do conceito de mobilidade de portadores de carga em semicondutores orgânicos, para estudar as interfaces entre eletrodos metálicos e semicondutores, e que inclui tanto SCLC e conceitos emissão termiônica. (2) Motivação e objetivo por detrás do uso de método SCLC para determinar as propriedades de transporte em P3HT. Em seguida é apresentado o método de fabricação e caracterização elétrica dos diodos para calcular os portadores de carga positivos e negativos no P3HT. Finalmente, resultados e discussões baseados em resultados obtidos dos dispositivos. (3) Introdução sobre o novo conceito de transistor COT. Seguido pelo método de fabricação e caracterização elétrica dos transistores e resultados e discussões baseados em resultados obtidos dos transistores.

Semicondutores orgânicos são úteis para uma ampla gama de aplicações, devido à sua combinação de propriedades eletrônicas e óticas de semicondutores com propriedades mecânicas e de processabilidade de polímeros. O Capítulo 1 apresenta uma visão geral das propriedades de semicondutores orgânicos. Estes têm muitas vantagens, tais como a fácil fabricação, flexibilidade mecânica, baixo custo, etc. No entanto, a limitação principal é a baixa mobilidade de portadores, o que dificulta as suas aplicações em que são necessários alta velocidade e desempenho. A baixa

mobilidade dos portadores é devida à desordem na morfologia que tende a localizar os estados eletrônicos e o transporte de carga ocorre através saltos entre esses estados localizados. A mobilidade caracteriza a facilidade com que a espécie carregada se move sob a influência do campo elétrico. Em semicondutores orgânicos, a mobilidade de carga dos portadores depende do campo elétrico aplicado e da temperatura. O Capítulo 1 destaca alguns dos modelos importantes que descrevem esta dependência. As propriedades de transporte dos portadores de carga de semicondutores orgânicos são usualmente analisadas por uma série de técnicas. Por exemplo, o tempo de voo (TOF), corrente limitada por carga espacial (SCLC), transistores de efeito de campo orgânicos, extração de carga por aumento linear de tensão (CELIV). Destes métodos, TOF é o mais popular para realizar medidas de mobilidade de transporte de materiais orgânicos. No entanto, muitas vezes TOF não é prático para avaliar a mobilidade dos materiais, uma vez que requer filmes com vários micrometros de espessura. É muitas vezes difícil de replicar a morfologia dos filmes finos usados nos dispositivos nos filmes espessos necessários para as medições de TOF. Como consequência, a mobilidade dos portadores de carga medida utilizando o método TOF em filmes com diversos micrometros de espessura poderia ser completamente diferente da mobilidade real em filmes finos de espessuras nanométricas, quando utilizado no dispositivo. Em nossa opinião, a técnica de SCLC é muito mais simples do que o método TOF, uma vez que não necessita de filme mais espesso e envolve custo experimental baixo.

O capítulo 2 estuda as interfaces entre eletrodos de metal e semicondutor intrínseco, nominalmente não dopado (não intencionalmente dopado) de semicondutores, com foco principal na corrente limitada por injeção (ILC) e SCLC. ILC ocorre quando o deslocamento entre a função de trabalho do metal e a energia do LUMO (HOMO) de semicondutores é suficientemente alta para causar uma má injeção de portadores de carga do metal para o semicondutor, devido à existência de uma barreira de energia. Um dos exemplos mais importantes é a emissão ILC Schottky. É um fenômeno em que o potencial de barreira entre a interface metal-semicondutor é reduzido, devido à combinação de campos elétricos aplicados e a força da imagem. Uma explicação detalhada pode ser encontrada no Capítulo 2 seção 4. Contrariamente ao ILC, SCLC ocorre quando a resistência de contato é muito menor do que a resistência do material agrupado. Em baixas tensões aplicadas, as características de corrente-tensão seguem a lei de Ohm, o que implica que a densidade de portadores livres gerados termicamente no interior dos filmes é maior

do que a dos portadores injetados. A densidade de corrente na região condutora é dada por  $J = qn_0\mu V/d$ , onde  $n_0$  é a concentração de elétrons livres no equilíbrio térmico (considerando-se apenas de elétrons),  $\mu$  é a mobilidade do portador de carga,  $V$  é a tensão aplicada e  $d$  é a espessura da amostra. Com o aumento da tensão, a densidade dos portadores injetados se torna comparável com a densidade de portadores livres gerados termicamente, o mecanismo SCLC torna-se perceptível e a curva corrente- tensão sofre alterações em suas características. Portanto, o início da SCLC tem lugar quando as características da corrente-tensão começam a passagem da lei de Ohm para o regime da SCLC. A tensão de início é dada por  $V_\Omega = 8/9(qn_0d^2/\epsilon)$  onde  $\epsilon$  é a permeabilidade absoluta do semiconductor. Com a continuação do aumento de tensão, mais elétrons (ou buracos) são injetados a partir do metal para o semiconductor. Devido à baixa mobilidade dos semicondutores orgânicos, estes elétrons são acumulados perto da interface metal-semiconductor e previnem mais injeção de elétrons. Em outras palavras, a corrente é limitada pela sua própria carga no espaço, o que por sua vez reduz o campo elétrico no eletrodo de injeção para zero. A blindagem devido a estas "catgas espaciais" produz características não lineares de corrente-tensão. Nesta região, a densidade de corrente,  $J = 9q\mu V^2/8d^3$  é dada pela lei de Mott-Gurney para o caso de tipo único de portadores e ausência armadilhas.

Resumindo, para a região condutora,  $J$  é proporcional a  $V^n$ , onde  $n$  é o coeficiente angular da curva ajustada, e no caso da região ôhmica  $n \approx 1$  e para da região SCLC  $n \approx 2$ . No, capítulo 2, seção 5, são derivadas as expressões matemáticas de densidade de corrente ôhmica, ponto de cruzamento e regiões SCLC. Além disso, um contato ôhmico (ou quase-ôhmico) na interface metal-semiconductor, é importante para ocorrer uma injeção de carga unipolar que permita medir a mobilidade do portador na região SCLC. A injeção unipolar pode ser obtida ajustando a diferença entre a função-trabalho do metal e a energia do LUMO (HUMO) do semiconductor orgânico, ver Capítulo 2 seção 6.

O objetivo deste projeto é a avaliação da mobilidade de portadores de carga positivas e negativas, ou seja, buracos e elétrons, respectivamente, o P3HT regio-regular (RR-P3HT), usando o método SCLC. Anteriormente, o método TOF foi usado para calcular as mobilidades dos portadores de carga no RR-P3HT, mas segundo nosso conhecimento, até agora só a mobilidade de portadores positivos foi calculada utilizando o método de SCLC. Finalmente, a comparação

também será feita com mobilidades obtidas anteriormente por TOF. Para avaliar a mobilidade dos portadores de cargas positivos, apenas a mobilidade de configuração de diodo é usado com RR-P3HT entre ITO / PEDOT: PSS e Al foi utilizada. O princípio básico de operação envolve a injeção de buracos do ITO/PEDOT:PSS no RR-P3HT enquanto forma uma barreira de injeção de elétrons, sendo esta uma barreira de alta energia potencial entre o nível de Fermi de Al e o LUMO do P3HT. Desta forma, apenas os buracos são injetados no RR-P3HT, tendo somente a medida das mobilidades de portadores de carga positivos. O capítulo 3 seção 5 explica o princípio de funcionamento dos diodos em detalhe. A análise do gráfico log-log das características de corrente  $\times$  tensão do diodo com ITO/PEDOT: PSS dá uma região ôhmica ( $n \approx 1$ ) e uma região SCLC ( $n \approx 2$ ) em tensões baixas e altas, respectivamente. Substituindo o valor de  $V_\Omega$  como a tensão do início de SCLC,  $V_\Omega = 8/9(qp_0d^2/\epsilon)$ , obtém-se o valor de  $p_0 = 1.68 \times 10^{16} \text{ cm}^{-3}$ . O próximo passo foi calcular a mobilidade dos buracos. A mobilidade pode ser calculada usando-se  $J = qp_0\mu_h V/d$  que dá um valor de  $\mu_h = 1,16 \times 10^{-4} \text{ cm}^2/\text{Vs}$  e para a região de SCLC a mobilidade de buracos pode ser calculada utilizando  $J = 9q\mu V^2/8d^3$  o que dá um valor de  $\mu_h = 1,35 \times 10^{-4} \text{ cm}^2/\text{Vs}$ . O capítulo 3 seção 6 cobre a parte dos cálculos.

Para avaliar somente a mobilidade de portadores de carga negativos, é usada uma configuração de diodo com RR-P3HT entre Al / CsO (de cima) e Al / CsO (inferior). O princípio básico de operação envolve a injeção de buracos de elétrons por cima, no Al/CsO como no RR-P3HT, enquanto forma-se uma barreira de injeção de buracos, sendo esta uma alta barreira de energia potencial entre o nível de Fermi do Al/CsO e HOMO do RR-P3HT. Desta forma só elétrons são injetados estão no RR-P3HT e a avaliação de mobilidades será somente de portadores de carga negativa. A análise das características de corrente  $\times$  tensão do diodo dá uma região ôhmica ( $n \approx 1$ ) e uma região SCLC ( $n \approx 2$ ) em tensões baixas e altas, respectivamente. Da tensão  $V_\Omega = 8/9(qn_0d^2/\epsilon)$ , obtém-se o valor de  $n_0 = 3,36 \times 10^{16} \text{ cm}^{-3}$ . A mobilidade no regime ôhmico pode então ser calculada usando-se  $J = qn_0\mu_e V/d$ , que dá um valor de  $\mu_e = 1,71 \times 10^{-9} \text{ cm}^2/\text{Vs}$  e para a região SCLC  $J = 9q\mu V^2/8d^3$ , o que dá um valor de  $\mu_e = 1,93 \times 10^{-9} \text{ cm}^2/\text{Vs}$ .

A conclusão tirada partir dos resultados acima é que, embora as concentrações de portadores de carga gerados termicamente para ambos os portadores são da mesma ordem de grandeza, , i.e.  $p_0 \approx n_0 \approx 10^{16} \text{ cm}^{-3}$  à temperatura ambiente, com base nos valores de mobilidade o transporte de portadores de carga positivas é muito mais eficiente do que os portadores de carga negativas no RR-P3HT. Observou-se que quando o RR-P3HT é exposto ao oxigênio e à água, a mobilidade dos portadores de carga negativa é reduzida em quatro ordens de grandeza, mas, curiosamente, a mobilidade dos portadores de carga positiva permanece quase inalterada.

O segundo objetivo objetivo deste trabalho é o de fabricar e caracterizar eletricamente o transistor COT. Para contornar o problema da baixa mobilidade dos semicondutores orgânicos, a aplicação de transistores orgânicos que necessitam de correntes de saída alta é realizada através da utilização de dispositivos em arquitetura vertical. Aqui, os portadores de carga se movem através do dispositivo perpendicularmente ao substrato e, portanto, tem que viajar distância da ordem da espessura do filme, tipicamente inferior a um micrômetro. O capítulo 4, seção 2, tem uma breve descrição dos transistores com base em materiais semicondutores em arquitetura vertical. Neste trabalho, o desempenho dos transistores é ainda melhorado usando uma família diferente de transistores que foram denominados como COT. O conceito básico do COT tira vantagem da baixa mobilidade dos portadores em polímeros condutores. Pelo nosso conhecimento, este conceito é completamente novo e nunca foi testado antes. Nele, polianilina sulfonada (Span), um polímero condutor auto-dopado, é utilizado como o semicondutor/condutor. Foi encontrado, usando a teoria funcional da densidade (DFT) que o LUMO e HOMO de SPAN estão em torno de 3,7 eV e 4,7 eV em relação ao nível de vácuo, respectivamente. Além disso, estados eletrônicos desocupados foram encontrados muito perto de 3,65 eV.

A fabricação de COT envolve a deposição de SPAN com uma espessura  $t$  é depositada por polimerização química no topo de Si tipo n. Depois Al por sublimação térmica como terminais fonte (S) e de controle (CT), com uma distância  $L$  entre os eletrodos foram depositados. A relação entre  $L$  e  $t$  é escolhida de forma que  $L \gg t$ .



A interface Al/SPAN é conhecida por formar um contato quase-ôhmico, ao passo que a SPAN/n-Si é conhecida por formar um contato Schottky. Sobre a aplicação do potencial reverso os elétrons são injetados a partir da fonte na SPAN. Devido à alta resistividade (medida pelo método de quatro pontas) e a baixa mobilidade dos portadores na SPAN, os elétrons se acumulam perto do contato de injeção. Com a pequena espessura da camada de SPAN, devido à repulsão eletrostática entre os portadores de carga injetados, elétrons tendem a espalhar-se ao longo da camada de SPAN na direção perpendicular à interface Al/SPAN. Estes elétrons acumulados tendem a preencher os estados eletrônicos desocupados da SPAN. A ocupação desses estados eletrônicos pode ser alta o suficiente para que os elétrons possam adquirir uma energia potencial suficiente para superar a barreira de energia Schottky na interface SPAN/n-Si. O campo elétrico presente na barreira Schottky então dirige os portadores de carga para o terminal n-Si. Portanto, o fluxo de elétrons pode ser amplificado pelo controle da quantidade de injeção de elétrons do Al para SPAN. Observamos também que o dispositivo pode ser otimizado através da variação do comprimento do canal e espessura da camada de SPAN. Com base nas características do dispositivo, foi observado que o ganho de corrente é quase quatro vezes mais elevado em comparação com outros transistores baseados em materiais orgânicos semicondutores em arquitetura vertical. No entanto, sofre de uma corrente de fuga elevada. Assim, mesmo sendo o COT útil para aplicações de baixa tensão, mas a corrente de fuga elevada pode causar elevada dissipação de energia.

# Acknowledgements

---

*This licentiate thesis is hopefully a step towards my final Ph.D. I could not have come this far on my own. I would like to take this opportunity to express my sincerest thanks to the following people:*

***Prof. Dr. Ivo A. Hümmelgen**, my award-winning professor, for giving me this opportunity to work in a constantly evolving field of science and for always being the source of inspiration.*

***Prof. Dr. Michelle**, **Prof. Dr. Marlus** and **Prof. Dr. Serbena**, the three Organic Electronic wiz's, for always taking the time to help, whatever the problem or question may be and for the valuable discussions. Zé, wanna play LFD2?*

***Prof. Dr. Regina** for helping me with Sulfonated polyaniline preparation and for the guidance.*

*The entire of group of **Organic Optoelectronic devices** ( at this date IVO, Michelle, Marlus, Serbena, Marcia, Bruno, Diana, Cris, Ana, Rafael and previous members including Wagner, Keli, Lucieli).*

*My family for always has been there for me even in long separation times.*

*Last, but not least, CNPQ for research grant.*

# Contents

---

<b>1. Introduction</b>	<b>1</b>
1. Organic Electronics	1
2. Properties of organic semiconductors	1
3. Conduction in small molecules and polymers	3
4. Charge transport in disordered organic semiconductors	5
5. Charge carrier mobility	6
6. Charge carrier mobility measurement methods	9
<b>2. Charge injection</b>	<b>11</b>
1. Introduction	11
2. Interface barrier formation	11
3. Contact barrier types	13
4. Blocking/injected limited current (ILC)	14
5. Space-charge-limited current (SCLC)	18
6. SCLC mobility	24
<b>3. Evaluation of transport properties in region-regular poly(3-hexylthiophene) using SCLC method</b>	<b>28</b>
1. Introduction	28

# Contents

---

<b>2.</b>	<b>Poly(3-hexylthiophene)</b>	<b>28</b>
<b>3.</b>	<b>Motivation</b>	<b>29</b>
<b>4.</b>	<b>Fabrication</b>	<b>30</b>
<b>5.</b>	<b>Principle of operation</b>	<b>32</b>
<b>6.</b>	<b>Results and Discussions</b>	<b>34</b>
<b>7.</b>	<b>Conclusions</b>	<b>39</b>
<b>8.</b>	<b>Future work</b>	<b>39</b>
<b>4.</b>	<b>Controlled-Overflow-Transistor (COT)</b>	<b>40</b>
<b>1.</b>	<b>Introduction</b>	<b>40</b>
<b>2.</b>	<b>Transistors based on semiconducting materials</b>	<b>41</b>
<b>3.</b>	<b>Motivation</b>	<b>44</b>
<b>4.</b>	<b>Self-doped sulfonated polyaniline (SPAN)</b>	<b>45</b>
<b>5.</b>	<b>COT fabrication</b>	<b>56</b>
<b>6.</b>	<b>Junction characteristics</b>	<b>58</b>
<b>7.</b>	<b>Results and Discussions</b>	<b>60</b>

# Contents

---

8.	Current gain	70
9.	Conclusions	72
10.	Future work	73

References	i
------------	---

# List of Figures

---

1. Scheme for the orbitals and bonds for two  $sp^2$ - hybridized carbon atoms, where  $\sigma$  - bonds are formed by overlapping of  $sp^2$  - orbitals and  $\pi$ - bonds are formed by side-to-side overlapping of  $p_z$ - orbitals 2
2. Simplified illustration of a polaron. As the electron moves through the organic material, it attracts positive ions. This lattice distortions travels with the electron. 3
3. Energy level shifts throughout the material because of the local disorder. LUMO and HOMO may be approximated by a Gaussian density of states. Hopping of electrons occurs through the LUMO (blue) and of holes through the HOMO (red). 6
4. Formation of interface energy barrier between a metal and an intrinsic semiconductor. The picture shows the formation of a contact barrier for the pure and defect free contacts. The energy barrier is given by  $\Phi_b = \Phi_M - \chi$ . 13
5. Shows two barriers types for an intrinsic semiconductor. Left picture:  $\Phi_M > \Phi_S$ , corresponds to an injection limited electron contact and an Ohmic hole contact. Right picture:  $\Phi_M = \Phi_S$ , corresponds to neutral contact. The energy barrier,  $\Phi_b$ , in these pictures shown for electrons given by  $\Phi_b = \Phi_M - \chi$ . 14
6. Band diagram at a metal/semiconductor contact. The straight solid line shows the band-tilt due to the external field, the dashed line shows the image charge potential and the thick line shows the sum of two, which is the actual profile of the potential as a function of  $x$ . 17
7. Shows a schematic representation of injection of electrons from a metal into an organic semiconductor of low mobility. Electrons are accumulated at the semiconductor side near the interface and screens further injection of electrons from the metal. 19
8. Current-voltage characteristics of Cu/CNCP/Al sample, Cu positively biased. Segments (a), (b) and (c) corresponds to increasing voltage, segment (d) corresponds to decreasing voltage. 24
9. Schematic figures of diodes with majority carriers as holes and electrons. In case of hole only device, only the metal with the higher work-function can inject holes provided that the opposite lying contact is not a good electron injecting contact. The opposite is true in the case of electron only device. 26

# List of Figures

---

10. Two different regio-regularities that can be incorporated into a polymer chain (B) The chemical representation of regio-regular poly(3-hexylthiophene) (P3HT). 28
11. Left picture shows ITO glass substrate with etched ITO from the sides, middle picture shows the mixture of spin-coated solutions of P3HT and PEDOT:PSS on top of ITO, right picture shows the evaporated Al electrodes with as active area of  $0.3\text{ cm}^2$ . 31
12. Schematic energy diagrams with respect to vacuum level for ITO (150 nm), PEDOT:PSS (100 nm), region-regular P3HT (100 nm), Al (150 nm), a hole-only single-carrier devices. Holes are collected via PEDOT:PSS of work-function  $\approx 5.2\text{ eV}$ , by positively biased ITO electrode with work-function  $\approx 4.9\text{ eV}$ . On the other hand, negatively biased Al with a work-function  $\approx 4.3\text{ eV}$  cannot inject electrons due to high energy barrier between its fermi level and LUMO of P3HT. 33
13. Schematic energy diagrams for Al (150 nm), CsO (5 nm), region-regular P3HT (100 nm), CSO (5 nm), Al (150 nm), an electron-only single-carrier device. 34
14. Inset figure shows the current-voltage characteristics of Al/P3HT/PEDOT:PSS/ITO diode with Al biased and PEDOT:PSS/ITO as grounded. Main figure shows the log-log plot of the inset figure with top contact Al/CsO negatively biased and bottom contact Al/CsO positively biased, respectively. At low voltages ( $V < 1\text{ V}$ ), an Ohmic region is observed and at higher voltages ( $V > 1\text{ V}$ ), SCLC region is observed. 35
15. Inset figure shows the current-voltage characteristics of Al/CsO (top)/P3HT/CsO/Al (bottom) diode with top Al/CsO biased. Main figure shows the log-log plot of the inset figure with top contact Al/CsO negatively biased and bottom contact Al/CsO positively biased, respectively. At low voltages ( $V < 1\text{ V}$ ), an Ohmic region is observed and at higher voltages ( $V > 1\text{ V}$ ), SCLC region is observed. 37
16. Lilienfeld's schematic drawing of the first current amplifier, (10), (11) marking the semiconductors and (12) a metal layer. 41
17. Energy band diagram of a MBT 42

# List of Figures

---

18. Different bases of polyaniline formed by oxidative and protonic doping with HA as acid proton donor. Undoped phase amine groups ( $-NH-$ ) contains non-bonding (lone pairs) nitrogen orbitals while imine groups ( $-N=$ ) contains a mixture of lone pairs and  $\pi$ -conjugated orbitals. 46
19. Semiconducting state of Sulfonated polyaniline 47
20. Formation of bipolarons 47
21. Conducting state of sulfonated polyaniline with no change in the number of electrons. The polarons separates, which results in a polaron lattice. 48
22. Schematic representation of deposition of SPAN on top of n-Si 51
23. SPAN thickness as a function of the amount of time (in hours) n-Si was in contact in the SPAN solution. 52
24. AFM 2D images of  $8 \times 8 \text{ nm}^2$  SPAN prepared using (A) 1:1 (B) 3:1 (C) 5:1 (D) 7:1 concentrations of metanillic acid and aniline. The images were using the dynamic mode. 54
25. Schematic figure of a linear four-point probe technique used to measure SPAN sheet resistance on top of a glass. 55
26. Schematic representation of a controlled-channel-overflow transistor using Al contacts as source and control-terminals and drain as n-type Si. 57
27. Density of electronic states of SPAN tetramer as a function of the energy with respect to the vacuum level. Inset: ground state geometry of the SPAN tetramer. 59
28. Electron only current of  $\text{Al}(-)/\text{SPAN}/\text{n-Si}/\text{Al}(+)$  and  $\text{Au}(-)/\text{SPAN}(+)/\text{n-Si}/\text{Al}(+)$  devices. 60
29. Schematic representation of a model with two parallel Schottky diodes between CT-D and S-D with its respective currents. 61
30. Schematic representation of the COT in the common-source configuration. 62



# List of Figures

---

31. Characteristic curves  $I_d(V_d)$  of the device ( $L = 45 \mu m$  and  $t = 200 nm$ ) for different  $V_{CT-S}$  ranging from 0 to 0.5 V. Inset: Device structure with the corresponding axes. 63
32. Schematic energy diagram of COT. 64
33. log-log plot of the  $I_d(V_d)$  data of Figure 30 for different  $V_{CT-S}$  in the range  $V_d < 1$ . The continuous line is a power-law fit to the experimental data with exponent 2. 66
34.  $\ln I$  versus  $V^{1/2}$  plot of Figure 42 for  $V_{CT-S} = 0 V$  and  $0.5 V$  in the range  $V_{D-S} > 1$ . The continuous lines are straight lines fitting to the experimental data. Inset: The linear coefficient of the continuous lines in  $\ln I$  versus  $V^{1/2}$  plot. 68
35. Schematic figure of electric field lines in the colors blue and black produced by the voltages  $V_{CT-S}$  and  $V_{D-S}$ , respectively. The additional effect in COT comes from the distribution of electric field lines produced by  $V_{CT-S}$  in  $x$  as well as  $y$  - direction. 69

# List of Tables

---

1. Compares the selected positive charge carrier ( $\mu_h$ ) and negative charge carrier ( $\mu_e$ ) mobilities values obtained using time-of-flight (TOF) and space-charge-limited-current (SCLC) methods. 30
2. Compares obtained values of the positive ( $\mu_h$ ) and negative ( $\mu_e$ ) charge carrier mobilities using SCLC method with the mobilities values obtained using time-of-flight (TOF) method. 39
3. Compares the common-emitter gain values of the metal-base, permeable-base and polymer space-charge-limited transistors. 45
4. The dependence of SPAN conductivity on the sulfonation degree. 49
5. Compares the common-emitter gain obtained with different  $L$  and  $t$  devices at  $V_D = 5V$  71
6. Comparisons of current gain achieved with different configurations of the transistors. 72

## LIST OF SYMBOLS AND ABBREVIATIONS

$A^*$	Richardson-Dushman constant
Al	Aluminium
Au	Gold
Alq3	Tris-(8-hydroxyquinoline) aluminium
Ca	Calcium
$C$	empirical constant for the disorder formalism
$C_0$	capacitance per unit area of parallel-plate capacitor
CELIV	Charge extraction by linearly increasing voltage
$c$	relative concentrations of traps
CNCP	conjugated non-conjugated alternating copolymer
$\text{Cs}_2\text{CO}_3$	caesium carbonate
CsO	caesium oxide
COT	Controlled-Overflow-Transistor
CT	control-terminal
D	drain terminal
$d$	thickness of the organic semiconductor material
DOS	Density-of-states
$dx$	infinitesimal distance along the $x$ -axis
$E_g$	band-gap energy
$E_C$	conduction band energy
$E_{FS}$	Intrinsic Fermi level of the semiconductor
$E_V$	valence band energy

$F$	electric force
Ge	Germanium
HCl	Hydrochloric acid
HOMO	highest occupied molecular orbital
H <sub>2</sub> SO <sub>4</sub>	sulfuric acid
H <sub>2</sub> NO <sub>3</sub>	nitric acid
HF	hydrofluoric acid
$I$	electric current
$I_e$	emitter current
$I_b$	base current
$I_c$	collector current
$I_D$	total drain current
$I_{S \rightarrow CT}$	current between S and CT
$I_{S \rightarrow D}$	current between S and D
$I_{CT \rightarrow D}$	current between CT and D
ITO	indium tin oxide
ILC	Injecting-limited current
$J$	current density
$J_{ILC}$	ILC current density
$K$	Boltzmann constant
LUMO	lowest unoccupied molecular orbital
MBT	Metal-base transistor
n	number density of free carriers
$V^n$	$n$ is the angular coefficient of the fitted curve

n-Si	n-type silicon
$n_0$	thermal equilibrium free electron concentration
$n_{i\text{ injected}}$	injected free-electron concentration
P3HT	poly(3-hexylthiophene)
PEDOT:PSS	poly(3,4-ethylenedioxythiophene) poly(styrenesulfonate)
PBT	Permeable-base transistor
PANI	polyaniline
$p_t$	trapped charges
$p$	free charges
$q$	elementary charge
$q\phi_{BE}$	energy barrier between emitter and base terminals
$q\phi_{BC}$	energy barrier between base and collector terminals
$Q_{i\text{ injected}}$	total injected charge per unit area
$Q_0$	total charge per unit area
RR	Regio-regular
Si	Silicon
S	source terminal
$\text{SO}_3^-$	sulfonate group
SPAN	Sulfonated polyaniline
SCLC	space-charge-limited current
T	absolute temperature
TOF	Time-of-flight
$U$	work done by electron in electric field
$V$	applied potential difference

$V_L$	vacuum level
$V_{\Omega}$	crossover voltage
$V_{CB}$	Collector-base voltage
$V_2O_5$	Vanadium pentoxide
$V_{CT-S}$	electrical potential difference between CT and S
$V_{D-S}$	electrical potential difference between D and S
$W$	depletion region
$x_{\max}$	maximum potential energy
$\Phi$	electrostatic potential
$\Phi_b$	potential energy barrier
$\Phi_M$	work-function of the metal
$\Phi_S$	work-function of the semiconductor
$\alpha$	common-base enhancement factor
$\beta$	common-emitter current gain
$\gamma$	field-dependence mobility
$\mathcal{E}_t$	discrete trap energy
$\varepsilon$	absolute permittivity of the semiconductor
$\varepsilon_0$	permittivity of free space
$\varepsilon_r$	relative permittivity of the material
$\theta$	trap-limiting factor
$\mu$	mobility
$\mu_0$	zero-field mobility
$\mu_{\infty}$	activation less mobility (or infinite temperature mobility)

$\mu_e$	electron mobility
$\mu_h$	hole mobility
$v_d$	Carrier drift velocity
$n$	number density of free carriers
$\rho$	Resistivity
$\rho_{injected}$	injected free charge concentration
$\sigma$	Electrical conductivity
$\Sigma, \omega$	Gaussian distribution widths
$\Delta$	activation energy
$\Delta\phi_B$	maximum potential energy
$\xi$	electric field
$\mathcal{E}_t$	discrete trap energy
$\varepsilon$	absolute permittivity of the semiconductor
$\varepsilon_0$	permittivity of free space
$\varepsilon_r$	relative permittivity of the material
$\chi$	electron affinity of semiconductor

# 1. Introduction

---

## 1. Organic Electronics

Over a century ago, Leo Baekland synthesized the first man made polymeric plastic, unique to anything previously known [1]. Since then, the scientific community has used organic materials in pharmaceuticals, kitchenware, insecticides, safety equipment's, etc. This is due to the fact that the overwhelming majority of organic materials are insulators and therefore, historically their functionality in electronics has been limited to electrical insulation. Electronic applications emerged over the last fifty years, first with Pope's study of the excited electronic structure of anthracene in 1960's [2], MacDiarmid, Shirakawa and Heeger achievement of doping polyacetylene with iodine to produce conducting polymers in 1970's [3], the use of organic semiconductors in xerography in the 1980's [4], and recently with the increase of consumer products utilizing organic materials for electronic purposes [5]. The field of electronics that emerged with the discovery of conducting and semiconducting organic (carbon) based-materials is known as Organic Electronics. It has been used in wide variety of applications including polymer solar cells [6], organic-based transistors [7] and organic light-emitting diodes [8].

## 2. Properties of organic semiconductors

This behavior as semiconductors can be understood by considering one of the simplest examples, polyacetylene. In polyacetylene exists a continuous network, often a simple chain, of adjacent unsaturated carbon atoms i.e. carbon atoms in  $sp^2$  - hybridization state where the  $sp^2$  - orbitals form a triangle within a plane and half-filled  $p_z$  - atomic orbital, are in the plane perpendicular to it. A  $\sigma$  - bond is formed by an overlap of two  $sp^2$  orbitals belonging to the neighboring carbon atoms. On the other hand, side-to-side  $\pi$  - overlap of the half-filled  $p_z$  - atomic orbitals leads to the formation of delocalized  $\pi$  - states (Figure 1).

---



---

## Introduction

---

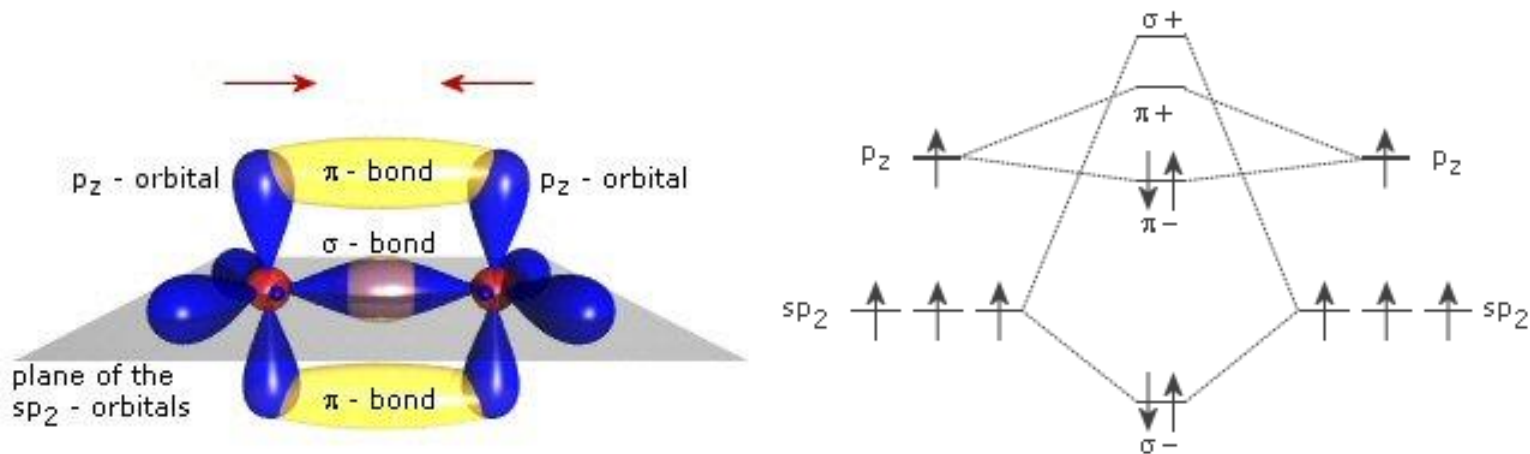


Figure 1: Scheme for the orbitals and bonds for two  $sp^2$ -hybridized carbon atoms, where  $\sigma$ -bonds are formed by overlapping of  $sp^2$ -orbitals and  $\pi$ -bonds are formed by side-to-side overlapping of  $p_z$ -orbitals [9].

The system of alternating double ( $\sigma$  and  $\pi$ ) bonds and single  $\sigma$ -bond in the conjugated backbone gives rise to a separation of bonding and anti-bonding states resulting in the formation of an energy gap and a spatially delocalized band-like electronic structure. The highest occupied molecular orbital (HOMO) consists of bonding states of the  $\pi$ -orbitals with filled electrons and is analogous to the valence band in silicon. The lowest unoccupied molecular orbital (LUMO) consists of empty higher energy anti-bonding ( $\pi^*$ ) orbitals and is analogous to the conduction band. The energy difference between LUMO and HOMO defines the band-gap energy,  $E_g$ , of the organic material.

Another important factor in determining the character of the electronic states is that the electrons and lattice are strongly coupled. As shown in Figure 2, an injected charge carrier will polarize the nearby region. The structural deformation of the area of the charged molecule follows the motion of the charge within the lattice almost instantaneously and remains spatially

limited to the nearby environment of each charged molecule. Since what is moving through the material is not simply a positive or negative charge carrier but also a local deformation, the charge carriers in organic semiconductors are referred to as polarons. Hence, terms like positive and negative charge carriers are more frequently used in organic semiconductors.

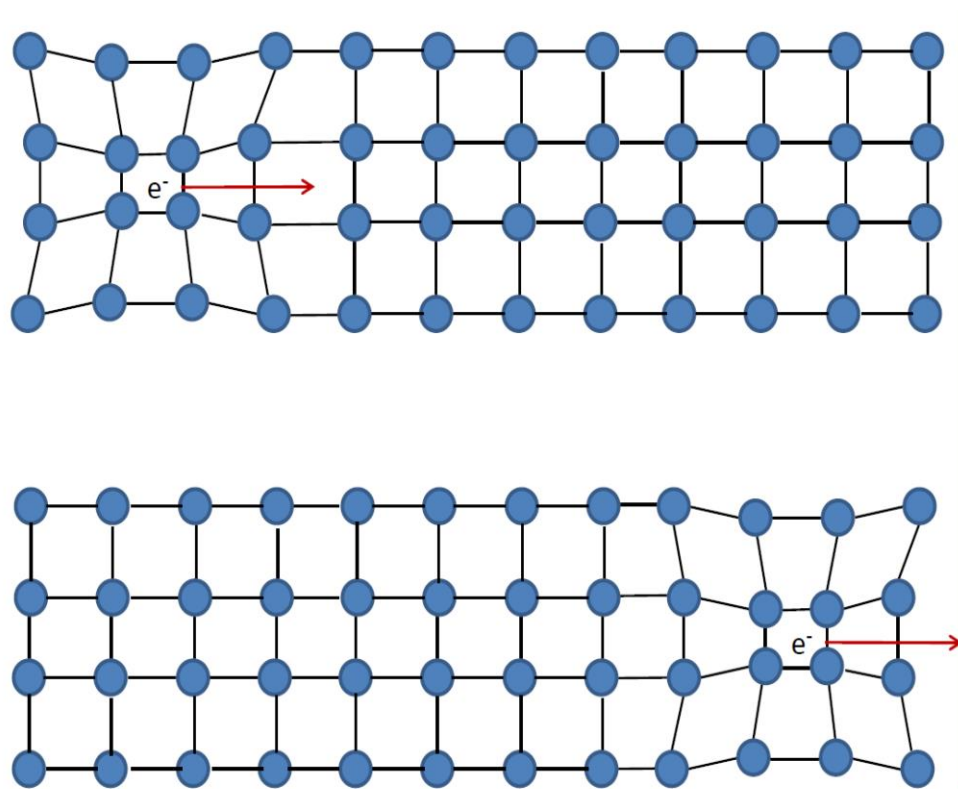


Figure 2: Simplified illustration of a polaron. As the electron moves through the organic material, it attracts positive ions. This lattice distortions travels with the electron.

### 3. Conduction in small molecules and polymers

Organic semiconductors can be arranged in order of increasing complexity: small molecules and polymers. Small molecule is a term broadly used to refer to those compounds with a well-defined molecular weight. In contrast, polymers are long-chain molecules consisting of an indeterminate number of repeating molecular units. A commonality of both the polymers and

## Introduction

---

organic molecules is a  $\pi$  - conjugated chemical structure. Polymers are usually quite long and their  $\pi$  - conjugation is interrupted by defect, hence the conjugated polymers can be considered as an assembly of conjugated segments. The length of the segments varies randomly and that is the main reason for energetic disorder implying inhomogeneous properties and a relatively broad density-of-states (DOS). The width of the DOS, to a large degree, determines the charge transport.

The major difference between organic semiconductors based on small molecules and conjugated polymers are the method of preparation. Thin films of small molecules are usually prepared by means of thermal sublimation, whereas for conjugated polymers a wide range of methods including spin-coating are available.

Some of the advantages of organic conjugated polymers and molecules are:

- The possibility of dissolving or emulsifying polymers in organic solvents to form inks to be used in the printing press. This ink can later be used for roll-to-roll solution based printing of electronics on flexible low-cost plastic substrates such as paper or plastic films. Several integrated circuits can easily be patterned onto these substrates, on large area with sufficient yield. This enables large-volume fabrication of electronics using cheap deposition methods (printing, casting);
- Usually, inorganic semiconductors such as silicon are hard and brittle materials and therefore require high temperatures (600 ° -1000° C) with precise control for uniform and crystalline deposition. On the other hand, organic semiconductors are soft (easily deformed) and flexible due to their weak bonding to neighboring molecules through Van der Waals forces. Therefore, they can be processed at room temperature, especially in the case of organic molecules;

- Tuning of material properties by chemical engineering, which enables endless opportunities;
- Organic materials can be made and integrated with other applications such as organic sensor device woven into textiles;

### 4. Charge transport in disordered organic semiconductors

In organic semiconductors, the charge transport (i.e. intramolecular transport) is easy along a conjugated chain due to the  $\pi$ -orbital overlap. However, due to the amorphous structure of polymer materials and the weak intermolecular interactions, charge transport between molecules (intermolecular transport) is difficult. An organic semiconductor often contains partially crystalline phases intermixed with partially amorphous phases. This disorder tends to localize the energy levels of states and the transport is produced by charge carrier hopping between these localized states (Figure 3). This localization and potential for collisions, scattering and delays contributes to relatively low mobilities of organic materials. Therefore, in spite of the above mentioned advantages, organic-based devices usually have lower performance due to their low mobilities. The following sections will shed a light on the concept of mobility in organic materials and highlight some of the popular methods that are employed to calculate it.

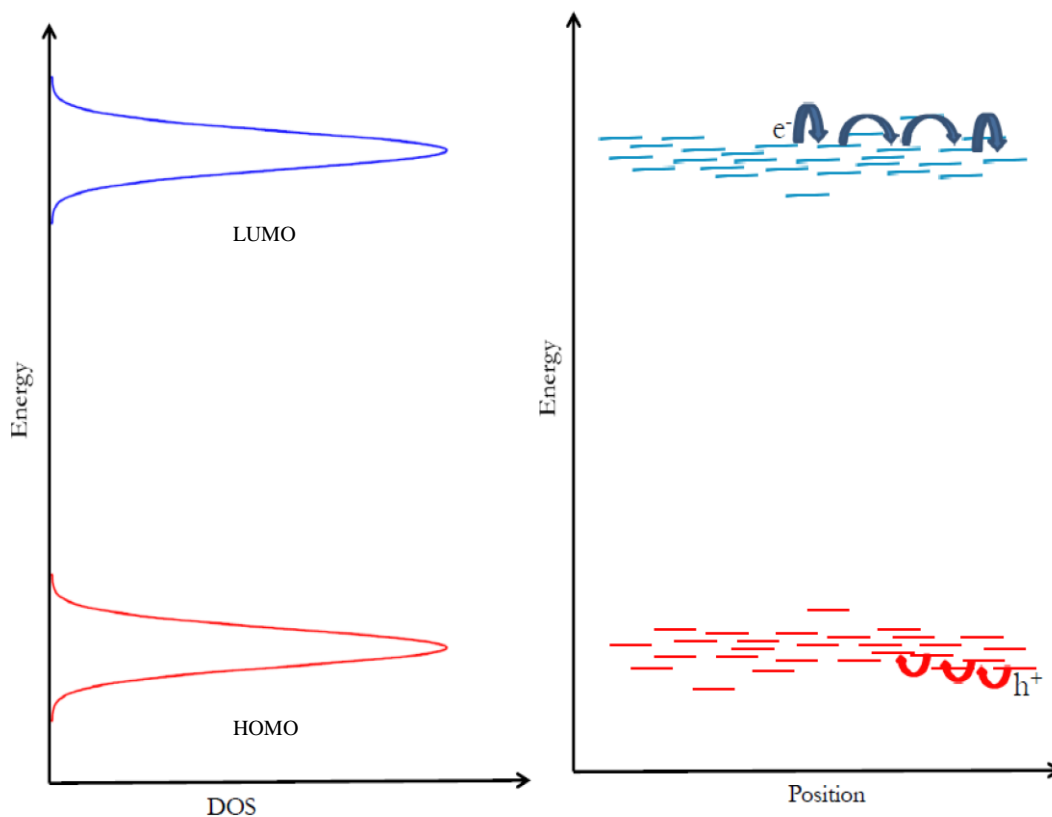


Figure 3: Energy level shifts throughout the material because of the local disorder. LUMO and HOMO may be approximated by a Gaussian density of states. Hopping of electrons occurs through the LUMO (blue) and of holes through the HOMO (red).

## 5. Charge carrier mobility

Electric current is the flow of charged particles, called charge carriers, which can be individual electrons, individual atoms or molecules. In the absence of external electric field, charge carriers will move randomly, especially in solid conductors, such as metals. As an electric field is applied charge carriers will be accelerated. In solids, collisions and scattering events limit this acceleration and result in a drift velocity for the carriers involved. In a given system, this velocity will vary depending on the driving force, in this case the electric field, applied. The

## Introduction

---

charge carrier mobility,  $\mu$ , is a measure of this proportionality between the carrier drift mobility,  $\nu_d$ , and the applied electric field,  $\xi$ :

$$\nu_d = \mu \cdot \xi \quad (1-1)$$

Typically, the carrier drift velocity is given in units of cm/s and the electric field or electric potential per unit distance in V/cm resulting in the mobility in units of  $\text{cm}^2/\text{Vs}$ .

Mobility is thus an indication of how fast charge carriers will flow in a medium as a function of electric field. This flow of charge carriers is the electric current. As an ability of a material to conduct electric current density,  $J$ , is measured by its electrical conductivity,  $\sigma$ , according to the following relation:

$$J = \sigma \cdot \xi \quad (1-2)$$

implying a relationship between charge carrier mobility and the electrical conductivity. As the carrier velocity is not the only factor in the flow of current, this relationship is given by:

$$\sigma = n \cdot q \cdot \mu \quad (1-3)$$

where  $n$  is the number density of charge carriers and  $q$  is the elementary charge (i.e. the charge of single electron or proton, or an ionized species with an excess or absence of one electron). Therefore, while the mobility informs how fast individual carriers will flow, the conductivity informs how fast net charge will flow and includes how many carriers are moving and the electrical charge of each carrier. The resistance of a material is measured by its resistivity,  $\rho$ , which is given in units of  $\Omega \cdot \text{m}$ . This resistivity is the inverse of conductivity. Thus, conductivity is measured in units of  $\Omega^{-1} \cdot \text{m}^{-1}$ .

Compare to the above theory, charge carrier mobility in disordered organic materials is known to be dependent on the applied field. Thus, the simple proportionality of

---

---

## Introduction

---

carrier drift velocity in Equation 1.1 does not hold, as the mobility itself is a function of the field. Instead, Poole-Frenkel dependence has been shown to be applicable to organic charge transport materials for fields from  $10^4$  to  $10^6$  V/cm [10, 11], despite some theoretical concerns about its applicability [11]. The Poole-Frenkel dependence of the mobility,  $\mu$ , on the electric field,  $\xi$ , is given by the following equation, where  $\mu_0$  is the prefactor or zero-field mobility and  $\gamma$  describes its field dependence:

$$\mu(\xi) = \mu_0 \exp(\gamma \sqrt{\xi}) \quad (1-4)$$

The most prominent model for fitting both the field and temperature dependence is Bassler's disorder formalism [12]. Here the disorders in both position including orientational effects and energy are considered to be Gaussian distribution with widths of  $\Sigma$  and  $\omega$ , respectively. The full expression is shown in equation (1-5) [12] with  $C$  as an empirical constant:

$$\mu(\xi, T) = \mu_\infty \exp\left[-\left(\frac{2\omega}{3KT}\right)^2\right] \exp\left\{C\left[\left(\frac{\omega}{KT}\right) - \Sigma^2\right]\xi^{1/2}\right\} \quad (1-5)$$

Finally, last factor is the composition. Extensive research work has been done on molecularly doped polymers and on how the mobility increases with higher content of the active species [13]. Trap-controlled transport has also been studied with higher concentrations and energetically deeper traps in transport material causing greater reductions in mobility [14, 15], as carriers are trapped more frequently and for longer amounts of time before being released (if released at all). In this case, the classic Hoesterey-Letson formalism [16] is used to describe the effects of mobility of a material with relative concentrations of traps,  $c$ , at a discrete trap energy,  $\varepsilon_t$ , below the majority material's energy level (HOMO or LUMO as relevant)

$$\mu(c) = \mu(c = 0) \frac{1}{1 + c \exp\left(\frac{\varepsilon_t}{KT}\right)} \quad (1-6)$$

As the concentration of traps rises, there is a transition to trap-to-trap transport, where some charge carriers will flow primarily in hops between traps and through the material.

## 6. Charge carrier mobility measurement methods

With the growth of organic electric fields, the understanding of the charge transport in disordered organic materials is thriving, but it is still a rather empirical quantity, as simulations are still insufficient to predict it a priori. Thus, it must be measured for all systems of interest to truly know its value. As the charge carrier mobility is a key parameter in understanding current motion in organic-based devices including the fastest response time of such a device, it is of great importance to the field. To determine charge carrier mobility in organic semiconductors, a number of methods have been employed including organic-field effect transistors [17], space-charge-limited-current (SCLC) [18], time-of-flight (TOF) [19] and charge extraction by linearly increasing voltage (CELIV) [20].

Of these methods, TOF method is the most popular one for charge carrier mobility measurements in organic materials. However, TOF is often not practical for evaluating the mobility of materials since it requires several micron thick films and specialized equipments. It is often difficult to replicate the morphology of the thin films in the devices (~ usually 10 nm) in the micron thick films required for TOF measurements. As a consequence, the charge carrier mobility measured using TOF method with several microns thick films could be completely different than the actual mobility encountered with nanometer thin films when used in the device. In our opinion, SCLC is a much simpler technique than the TOF method since it does not require thicker films and involves simple experimental setup.



## Introduction

---

The basic concept of SCLC will be explained in chapter 2 with help of metal-semiconductor interfaces. It is followed by using SCLC method to calculate positive and negative charge carrier mobilities in an organic semiconductor named poly(3-hexylthiophene) (P3HT) in chapter 3.

## 2. Charge injection

---

### 1. Introduction

In this chapter, firstly, we will have a glance at the interface barrier formation between metal and intrinsic semiconductor, undoped (only unintentionally) semiconductor. Secondly, various contact barrier types with respect to intrinsic semiconductor will be discussed. Finally, injection-limited current (ILC) and space-charge-limited current (SCLC) mechanisms will be reviewed.

### 2. Interface barrier formation

The basic definition of an interface energy barrier is the energy offset between the Fermi energy of the metal and the LUMO (HOMO) band-edge of semiconductor, where the majority carriers reside. Figure 4 shows the formation of metal-semiconductor contact for an intrinsic semiconductor assuming that both materials are pure and the interface is a defect free one. Before contact (left picture of Figure 4), the two systems are in the original state. The semiconductor has a conduction band level  $E_C$  at  $\chi$  from the vacuum level  $V_L$ , where  $\chi$  is the electron affinity. The Fermi-level  $E_{FS}$  is located halfway the band gap. The work-function of the semiconductor is defined as the distance of the semiconductor Fermi-level from the vacuum level,  $\Phi_S = V_L - E_{FS}$ . The energy difference between the valence band level  $E_V$  and the conduction band energy  $E_C$  is the band gap energy  $E_g$ ,  $E_V = E_C - E_g$ . The work-function of the metal is denoted as  $\Phi_M$  and equals the distance of the metal Fermi-level  $E_F$  to the vacuum level,  $\Phi_M = V_L - E_F$ . *It should be noted that energies are represented in eV throughout this thesis.*

---

## Charge injection

---

We will now focus on the formation of the interface barrier due to the energy offsets between the metal Fermi-level and semiconductor conduction band level. Upon contact, the Fermi- levels of the metal and semiconductor line out (right picture in Figure 4). When the work- function of the metal is smaller ( $\Phi_M < \Phi_S$ ), electrons can lower their energy by flowing from the metal into the semiconductor to shift its Fermi-level (accumulation). When the work-function of metal is larger, ( $\Phi_M > \Phi_S$ ), electrons will flow from the semiconductor into the metal, lowering the semiconductor Fermi-level (depletion). The latter case is shown in Figure 4. When the metal and semiconductor are contacted, there is a formation of depletion region,  $W$ , in semiconductor due to conduction electrons moving from semiconductor to the metal, leaving uncompensated positive donors behind. The depletion region does not contain mobile charges so that there can be an electric field. This depletion layer also acts like a potential barrier,  $\Phi_b$ . This barrier has a height of  $\Phi_M - \chi$ .for electrons to flow from the metal to the semiconductor. The size of the barrier for electrons moving from semiconductor to metal is  $\Phi_M - \Phi_S$ , which is also the equal to the total downward displacement of the bands in the semiconductor from the metal-semiconductor interface. It is also observed from Figure 4 that far from the contact, the semiconductor tries to establish the original state, as it was before contact.

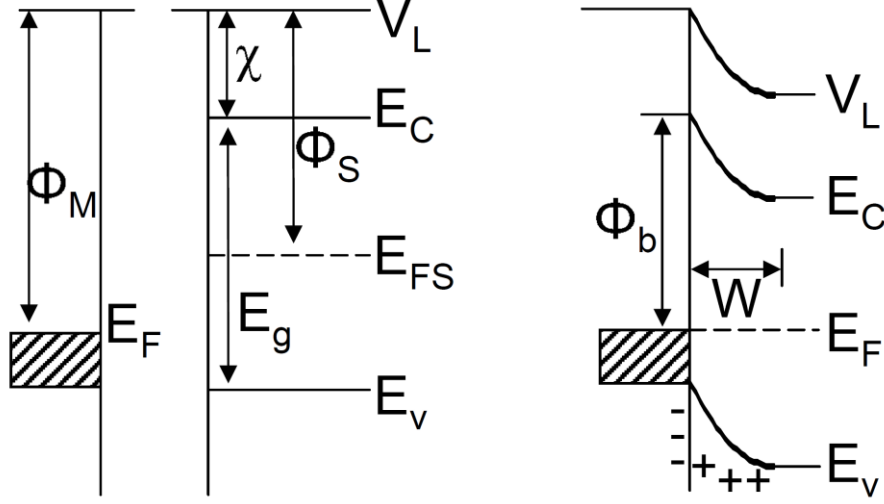


Figure 4: Formation of interface energy barrier between a metal and an intrinsic semiconductor. The picture shows the formation of a contact barrier for the pure and defect free contacts. The energy barrier is given by  $\Phi_b = \Phi_M - \chi$  inspired from [21].

### 3. Contact barrier types

In Figure 5, two essentially different contacts are described for an intrinsic semiconductor: (1) when the contact work-function is larger than the semiconductor work-function ( $\Phi_M > \Phi_S$ ), the electrons are depleted from the semiconductor, as discussed in the previous section. Due to the electron-depletion, the contact region cannot supply enough charge carriers to the bulk of the semiconductor, and the contact is called blocking or injection-limited for electrons. At the same time, the contact region contains an excess of holes (left picture of Figure 5). As a result, the contact region can supply charge flow demanded by the bulk of the semiconductor and the contact is Ohmic or bulk-limited for holes (2) When  $\Phi_M = \Phi_S$  (right picture of Figure 5), the Fermi-levels are aligned, and no charge redistribution is present. This is called neutral contact: both the electron and hole contact have an interfacial concentration of charge equal to their intrinsic free carrier concentration. (3) When the contact work-function is smaller

than the semiconductor work-function ( $\Phi_M < \Phi_S$ , not shown in Figure 5), the situation is reversed from (1): electrons are accumulated in the semiconductor, and the electron contact is Ohmic. The hole contact now becomes injection-limited.

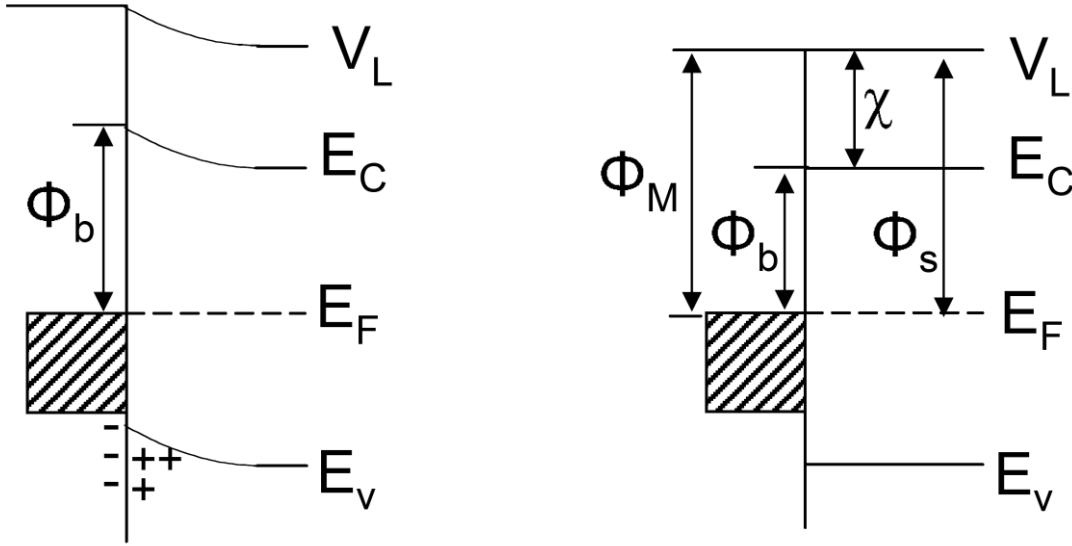


Figure 5: Shows two barriers types for an intrinsic semiconductor. Left picture:  $\Phi_M > \Phi_S$ , corresponds to an injection limited electron contact and an Ohmic hole contact. Right picture:  $\Phi_M = \Phi_S$ , corresponds to neutral contact. The energy barrier,  $\Phi_b$ , in these pictures shown for electrons given by  $\Phi_b = \Phi_M - \chi$  inspired from [21].

#### 4. Blocking/injection limited current (ILC)

ILC occurs when the energy offset between metal work-function and LUMO (HOMO) levels of organic semiconductor is sufficiently high to cause a poor injection of charge carrier from the metal to the semiconductor. In this case, the amount of injected charge is too small to give a significant bending of the electrostatic potential,  $\Phi$ . Therefore, the electric field in injection-limited devices is uniform. The electrostatic potential is defined by

---

## Charge injection

---

$$-\frac{d\phi}{dx} = \xi \quad (2-1)$$

where  $\xi$  is the electric field and  $dx$  is the infinitesimal distance along the  $x$ -axis. Since the focus here is on the conduction band and therefore we have chosen the value of electrostatic potential times charges equal energy of the conduction band with respect to the Fermi-level of the system:  $q\phi = E_C - E_F$ . The ILC current density,  $J_{ILC}$ , is a function of this electric field,  $\xi$ , and is expressed as:

$$J_{ILC} = J(\xi) = J\left(\frac{V}{d}\right) \quad (2-2)$$

where  $V$  applied voltage and  $d$  is the thickness of the organic material.

Generally, the field-enhanced thermionic emission model is used to represent the injection current from metal to the organic material through the Schottky barrier. The phenomenon in which a potential barrier is lowered due to the combination of applied electric field and the image force is called Schottky effect or field-enhanced thermionic emission. Consider an emitted charge from the metal into the semiconductor, at a distance  $x$  from the metal surface. An image charge will be induced in the metal, of opposite charge and equal distance  $-x$  from the surface. The electrostatic attractive force between the electron and the image charge is

$$F_{image} = \frac{-q^2}{4\pi(2x)^2 \epsilon} = \frac{-q^2}{16\pi x^2 \epsilon} \quad (2-3)$$

## Charge injection

---

where  $x$  is the distance electron-metal interface,  $q$  is the elementary charge and  $\varepsilon$  is the absolute permeability of the semiconductor,  $\varepsilon = \varepsilon_0 \varepsilon_r$  with  $\varepsilon_0$  as the permittivity of free space and  $\varepsilon_r$  as the relative permittivity of the material. As a result, apart from the work done by electron in the electric field,  $U = -q\xi x$ , there is an extra amount of work done by an electron in the course of its transfer from infinity to the point  $x$  given by  $U(x) = \int_{\infty}^x F dx = -\frac{q^2}{16\pi\varepsilon x}$ . The resulting potential energy of the electron (or hole for the case of hole injection) as measured from metal Fermi-level is

$$U(x) = -\frac{q^2}{16\pi\varepsilon x} - q\xi x \quad (2-4)$$

The position where the potential energy would be maximum,  $x_{\max}$ , can be obtained by differentiating (2-4) with respect to  $x$  ( $d[U(x)]/dx = 0$ ), which yields

$$0 = \frac{q^2}{16\pi\varepsilon x_{\max}^2} - q\xi \quad (2-5)$$

$$x_{\max} = \sqrt{q/16\pi\varepsilon \xi} \quad (2-6)$$

The maximum potential energy corresponding to  $x = x_{\max}$  can now be obtained from (2-4), as

$$U_{\max} = -q \left[ \frac{q\xi}{4\pi\varepsilon} \right]^{1/2} = -q\Delta\phi_B \quad (2-7)$$

Thus, under the presence of external electric field, the maximum potential energy is lowered by  $\Delta\phi_B$  (Figure 6).

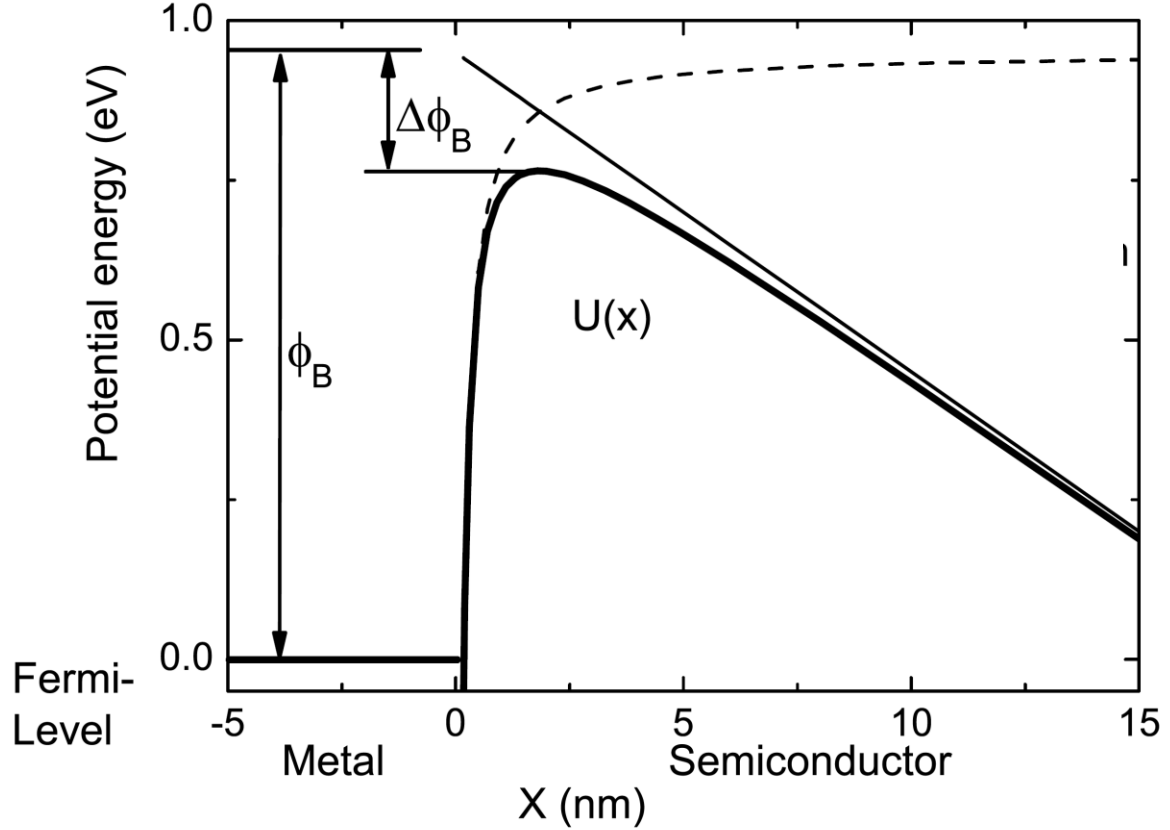


Figure 6: Band diagram at a metal/semiconductor contact. The straight solid line shows the band-tilt due to the external field, the dashed line shows the image charge potential and the thick line shows the sum of two, which is the actual profile of the potential as a function of  $x$  (equation 2-4) inspired from [22].

The current flow due to the Schottky effect can be represented by the Richardson-Dushman equation [23]



---

### Charge injection

---

$$J = A^* T^2 \exp \left[ - \frac{q\phi_b - \frac{1}{2} \beta \sqrt{\xi}}{KT} \right] \quad (2-8)$$

where  $A^*$  is the Richardson-Dushman constant,  $T$  is the absolute temperature,  $K$  is the Boltzmann's constant and  $\beta$  is a material constant given by

$$\beta = \sqrt{\frac{q^3}{\pi \epsilon}} \quad (2-9)$$

Taking the natural logarithm of (2-8), we can write the characteristic equation for Schottky emission as:

$$\ln J = \frac{1}{2} \frac{\beta \sqrt{\xi}}{KT} + \ln [A^* T^2] - \frac{q\phi_b}{KT} \quad (2-10)$$

Based on (2-10), the following three conditions should be satisfied in a device that exhibits the Schottky effect: (a) A plot of  $\ln J$  versus  $\sqrt{\xi}$  yields a straight line; (b) The slope of line should be equal to the theoretically calculated value of  $\beta/2KT$ ; (c) The variation of current with temperature should be predicted by (2-8);

## 5. Space-charge-limited current (SCLC) (Ohmic-to-bulk limited process)

Contrary to ILC, SCLC occurs when the contact resistance is much lower than the resistance of the bulk material. As electrons are emitted from the metal to the semiconductor, a space charge

---

## Charge injection

---

region develops at the semiconductor side due to the low mobility of organic semiconductors. This space charge causes a repulsive effect on the further injection of the electrons from the metal. The injected electrons must overcome both the attractive forces of the lattice (work-function) of the metal and repulsive forces of the space charge to flow to semiconductor. Figure 7 shows a schematic representation of the metal-organic material interface with the presence of space-charge region at the organic semiconductor side.

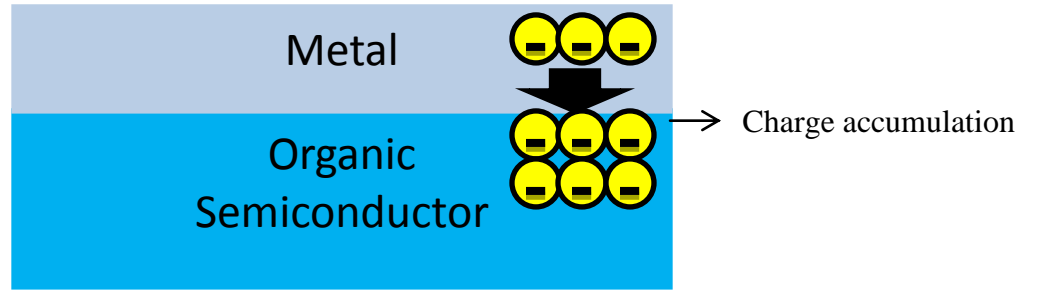


Figure 7: Shows a schematic representation of injection of electrons from a metal into an organic semiconductor of low mobility. Electrons are accumulated at the semiconductor side near the interface and inhibit further injection of electrons from the metal.

Figure 8 illustrates the typical current-voltage characteristics for one-carrier SCLC injection into a material. The SCL current-voltage characteristics are typically illustrated in log-log plot because the SCL and voltage has a power law relationship. At small voltage, segment (a) of Figure 8, the SCLC is not noticeable and Ohm's law dominates the current-voltage characteristics due to the presence of thermal equilibrium free carriers. The current density is expressed in terms of drift current (neglecting diffusion term of the current) as:

$$J = qn_0\mu\xi = qn_0\mu\frac{V}{d} \quad (2-11)$$

---

## Charge injection

---

where  $n_0$  is the thermal equilibrium free electron concentration (considering electron only),  $\mu$  is the charge carrier mobility,  $V$  is the applied voltage and  $d$  is the thickness of the specimen. As the voltage increases, there is no significant departure from Ohm's law until the average injected excess free-electron concentration,  $n_{injected}$ , becomes large enough to be noticeable. When  $n_{injected}$  becomes comparable to  $n_0$ , the space-charge-limited (SCL) mechanism becomes noticeable and the current-voltage characteristics changes. Therefore, the onset of SCLC takes place when the current-voltage characteristics begin to crossover from Ohm's law to SCLC regime. The voltage at which this crossover occurs is the crossover voltage,  $V_\Omega$ .

The total charge density into the semiconductor is given by

$$Q_{injected} = \rho_{injected} d = qn_{injected} d \quad (2-12)$$

where  $\rho_{injected}$  is injected free charge concentration and  $Q_{injected}$  is total injected charge per unit area. As stated above, the crossover voltage,  $V_\Omega$ , is the voltage when  $n_{injected} = n_0$ . Therefore,

$$Q_{injected} = qn_0 d \quad (2-13)$$

If we consider organic semiconductor is sandwiched between two metals, then the total charge per unit area,  $Q_0$ , on one plate of the parallel-plate capacitor is proportional to the applied voltage,  $V$ , across the capacitor, which can be written as:

$$Q_0 = C_0 V \text{ and } C_0 = \epsilon/d \quad (2-14)$$

---

---

### Charge injection

---

where  $C_0$  is the capacitance per unit area of parallel-plate capacitor. From (2-12),  $Q_{injected} = qn_0d = CV_\Omega = (\varepsilon/d)V_\Omega$ , by solving (2-13),  $V_\Omega$  can be written as

$$V_\Omega = (qn_0d^2/\varepsilon) \quad (2-15)$$

where C is the capacitance of the device. By inserting a factor of 8/9, we get:

$$V_\Omega = \frac{8}{9}(qn_0d^2/\varepsilon) \quad (2-16)$$

As the voltage increases further, more electrons are injected from metal to semiconductor. Due to the low mobility of organic semiconductors; these electrons are accumulated near the metal-semiconductor interface and prevent further injection of electrons (Figure 7). In simple words, the current is limited by its own space-charge, which in turn reduces the electric field at the injecting electrode to zero. The screening due to these “space-charges” produces non-linear current-voltage characteristics, segment (b) of Figure 8. The current density,  $J$ , in the SCLC can be obtained by starting from the expression of the drift current and Gauss’s law, we have:

$$J = qn\mu\xi \text{ and } \frac{d\xi}{dx} = \frac{qn}{\varepsilon} \quad (2-17)$$

where  $n_0 = n + n_{injected}$ . We can eliminate  $n$ , yielding:

---

### Charge injection

---

$$\frac{J}{\epsilon\mu} = \xi \frac{d\xi}{dx} \quad (2-18)$$

Integrating this expression from 0 to  $x$ , while assuming electric field to 0 at  $x = 0$  one obtains:

$$\frac{Jx}{\epsilon\mu} = \frac{\xi^2}{2} \text{ or } \xi = \sqrt{\frac{2xJ}{\epsilon\mu}} \quad (2-19)$$

Integrating once again over the thickness of the semiconductor from  $x = 0$  to  $x = d$ , one finds:

$$V = \int_0^d \xi dx = \sqrt{\frac{2J}{\epsilon\mu}} \frac{d^{3/2}}{3/2} \quad (2-20)$$

from which one obtains the expression for the SCLC as:

$$J = \frac{9\epsilon\mu V^2}{8d^3} \quad (2-21)$$

Equation (2-21) is known as the Mott-Gurney law for single-type of carriers and no traps and Child's law for solids [24]. This square law is the reason why the SCLC characteristics are typically shown on log-log plot. Based on (2-21), the following two conditions should be satisfied in a device that exhibits the SCLC phenomenon: (a) A plot of  $\ln J$  versus  $\ln V$  should

---

yield a region of slope equal to 2; (b) A plot of  $\ln J$  versus  $d$  should yield a region of slope equal to - 3. It is also important to note that equation (2-21) is for a trap-free case i.e. with the absence of traps in the semiconductor. In the case of traps, the current density equation is modified by a trap-limiting factor  $\theta$  relating to the proportion of trapped charges ( $p_t$ ) to free charges ( $p$ ) by

$$J = \frac{9}{8} \epsilon u \theta \frac{V^2}{d^3} \quad (2-22)$$

$$\text{where } \theta = \frac{p}{p + p_t}$$

For a trap-free case,  $p_t = 0$  and therefore  $\theta = 1$ ; with traps present,  $\theta$  is always less than unity. *Throughout this thesis, equation (2-21) will be used to calculate the mobility of semiconductor in the SCLC region by assuming  $\theta \approx 1$ .*

With further increase in voltage, the injected charges are no more affected by space-charges in the semiconductor since injected carriers become dominant process and the mobility is assumed as band mobility, see segment (c) of Figure 8. We won't explore this segment since it is not the focus of this thesis. A good explanation of the basic SCLC theory can be found in [24] by M. A. Lampert and P. Mark.

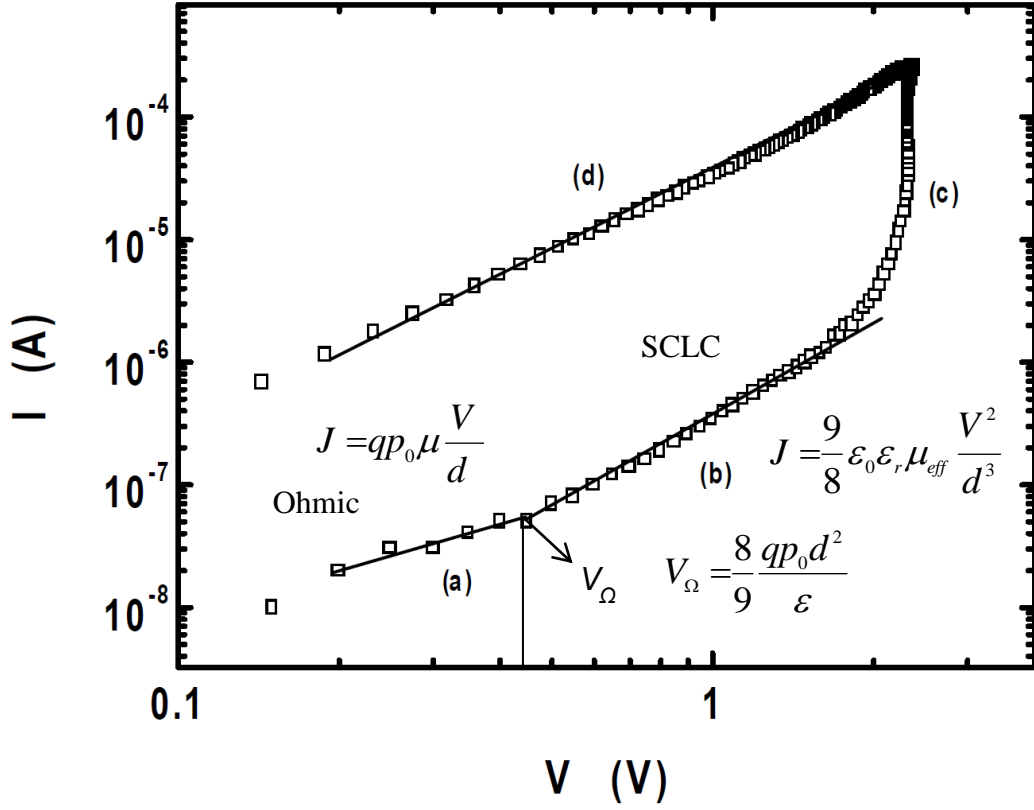


Figure 8: Current-voltage characteristics of Cu/CNCP/Al sample, Cu positively biased where CNCP stands for conjugated non-conjugated alternating polymer. Segments (a), (b) and (c) corresponds to increasing voltage, segment (d) corresponds to decreasing voltage, taken from [25].

## 6. SCLC mobility

As previously stated in Chapter 1, one of the methods of determining charge carrier mobilities in organic semiconductor is by using SCLC technique. The mobility in the SCLC regime is determined from the electrical characterization of a diode produced by sandwiching an organic layer of interest between two metal electrodes. The choice of electrodes is made in such a way that only quasi-unipolar (only positive or negative) charge carriers are injected into the active layer.

## Charge injection

---

Left picture of Figure 9 shows the energy scheme of a positive charge carrier-only device. On one side, a metallic contact with a high work-function is chosen in such a way that the difference between work-function of the metal and energy of the HOMO level of semiconductor is almost negligible. On the opposite lying contact, a blocking/injection-limited contact is formed between the work-function of the metal and the energy of the LUMO level of semiconductor with a potential energy barrier,  $\Phi_b$ . With positively-biased, the metal with higher work-function can inject positive charge carriers in the HOMO of the semiconductor. Due to the low mobility in disordered semiconductors, the desired carriers that are injected from the electrical contacts begin to build up “space-charge”, as previously discussed. On the other hand, the negatively-biased metal will have negligible injection of electrons due to the high potential energy barrier,  $\Phi_b$ , between work-function of the metal and the energy of the LUMO level of semiconductor. The opposite is true if one fabricates an electron only device shown in right picture of Figure 8. Therefore, to evaluate the carrier mobility using SCLC method two requirements must be fulfilled: (a) Quasi-Ohmic contact at the metal-semiconductor interface and (b) Unipolar charge injection.



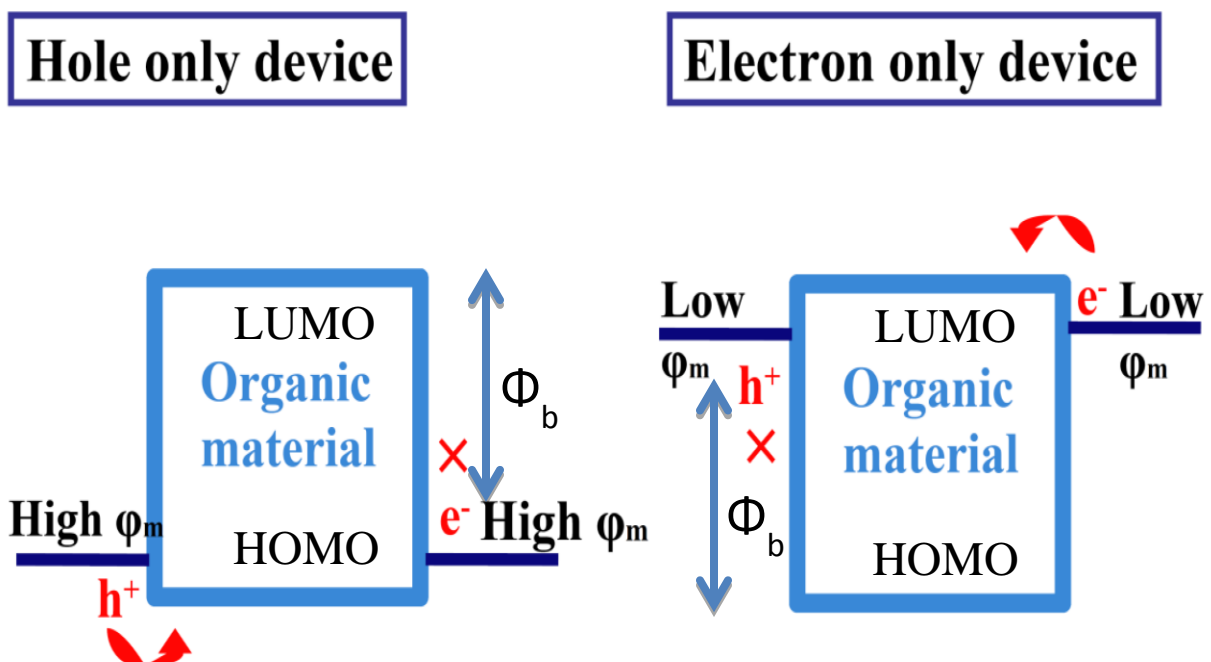


Figure 9: Schematic figures of diodes with majority carriers as holes and electrons. In case of hole only device, only the metal with the higher work-function can inject holes provided that the opposite lying contact is not a good electron injecting contact. The opposite is true in the case of electron only device.

One of the fundamental differences between organic-on-metal and metal-on-organic interfaces is that the former is usually formed by depositing the organic semiconductor by evaporation or by spin coating on a metal that has been exposed to atmosphere and is therefore somewhat contaminated: contaminants include hydrocarbons or residual solvent molecules that may be present due to the processing conditions. This contaminant layer effectively passivates the metal surface, and reduces the interaction between the organic molecules and metal, leading to an energy band alignment that is close to the Schottky-Mott limit.

In contrast, metal-on-organic contacts are usually deposited by metal evaporation in vacuum, where the presence of contaminants is greatly reduced. The stronger interaction between the organic surface and the metal often induces a strong Fermi-level pinning and a large

## Charge injection

---

interface dipole, causing the energy band alignment to depart from the vacuum level alignment expected from the electronic structure of the isolated metal and semiconductor.

Data analysis is done by fitting  $J$ - $V$  curves in the linear region (Ohmic region) and the quadratic region (SCLC region), respectively. Generally, for Ohmic region,  $J$  is proportional to  $V^n$ , where  $n$  is the angular coefficient of the fitted curve and in the case of Ohmic region  $n \approx 1$ . For SCLC region,  $J$  is proportional to  $V^n$ , where  $n \approx 2$ . Also, the value of  $V_\Omega$  can be obtained by the crossover point from Ohmic to SCLC regions. With the known value of  $V_\Omega$  and semiconductor thickness and absolute permittivity one can calculate the value of  $n_0$  using (2-15). The knowledge of the value of  $n_0$  can then be utilized to evaluate the charge carrier mobility in the Ohmic region, which can be evaluated using (2-11). Similarly, the value of charge carrier mobility in SCLC region can be evaluated by fitting of the SCLC region and utilizing (2-21).

### 3. Evaluation of transport properties in region-regular poly(3-hexylthiophene) using SCLC method

---

#### 1. Introduction

This chapter firstly gives a short introduction about regio-regular poly(3-hexylthiophene) (RR-P3HT) and its properties. Secondly, the main motivation behind this project is discussed. Next, fabrication, principle of operation and results based on the devices that are used to evaluate the transport properties in RR-P3HT will be reviewed. Finally, conclusions based on the obtained results and a glance at future work will be given.

#### 2. Poly(3-hexylthiophene)

Poly(3-hexylthiophene) (P3HT) is one of the most studied semiconducting polymer due to its high hole mobility, good solubility and processability [26]. It is stable both in doped and undoped state. The 3-hexyl substituent in the thiophene ring can be incorporated into the polymer chain with two different regio-regularities [27], shown in Figure 10 (A): head-to-tail (HT) and head-to-head (HH). A regio-random P3HT consists of both HH and HT in a random pattern while a regio-regular (RR) P3HT has only one kind of 3-hexylthiophene either HH or HT (Figure 10 (B))

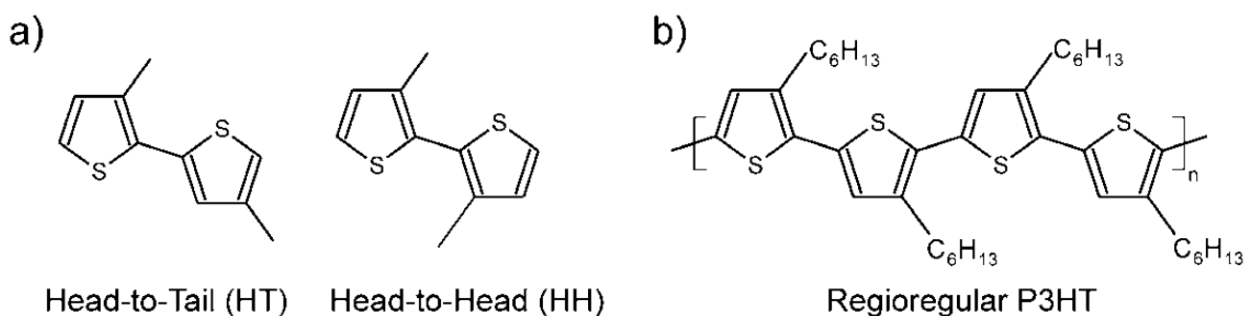


Figure 10: (A) Two different regio-regularities that can be incorporated into a polymer chain (B) The chemical representation of regio-regular poly(3-hexylthiophene) (P3HT) [27].

Upon casting onto thin films, RR-P3HT has great potential as an organic semiconductor in electronics because of its strong tendency to self-assemble into crystallites with ordered structures. This gives rise to positive charge carrier field-effect mobilities of the order  $0.1 \text{ cm}^2/\text{Vs}$  [28]. On the other hand, the regio-random P3HT has a twisted chain conformation with poor packing and low crystallinity, resulting in positive charge carrier field-effect mobilities of only  $10^{-4} \text{ cm}^2/\text{Vs}$  [27]. Depending upon the processing conditions and regio-regularity of the polymer, the polymer chains can be ordered in two different orientations, parallel or normal to the substrates [28]. The mobilities had been found to be three orders of magnitude higher when  $\pi$  – stacking direction is parallel to the direction of charge transport, thus demonstrating fast and efficient interchain transport of the carriers. The morphology and charge transport of the RR-P3HT has also been shown to depend on the molecular weight [29]. In addition, the choice of solvents strongly influences the microscopic morphology of the film and thus its mobility [26]. It has been established in the literature that the P3HT oxygen is known to form a charge transfer complex resulting in p-doping of P3HT [30]. Furthermore, oxygen induced degradation of P3HT is reported in decreased mobilities and increased trap densities [31].

### 3. Motivation

In the past, the charge carrier mobilities in P3HT has been evaluated using TOF method [32]. In this report, they claimed that by using a high purity and chemical/structural regularity a relatively high negative and positive charge carrier mobility in RR-P3HT can be obtained. To our knowledge, till now SCLC method has only been employed to evaluate the positive charge carrier mobility in P3HT [33]. The aim of this project is to evaluate both positive and negative charge carrier mobility in RR-P3HT using SCLC method and then to compare it and analyze the obtained results with the TOF results. Table 1 below compares the selected charge carrier mobilities obtained by TOF and SCLC methods.

## Evaluation of transport properties in RR-P3HT

	Methods		
Mobilities ( $\text{cm}^2/\text{Vs}$ )	TOF [32]	SCLC [33]	SCLC (this work)
$\mu_h$	$3 \times 10^{-4}$	$10^{-5} - 10^{-4}$	?
$\mu_e$	$1.5 \times 10^{-4}$	—	?

Table 1: Compares the selected positive charge carrier ( $\mu_h$ ) and negative charge carrier ( $\mu_e$ ) mobilities values obtained using time-of-flight (TOF) and space-charge-limited-current (SCLC) methods.

## 9. Fabrication

The devices characterized here have the metal/polymer/metal structure in a diode architecture prepared on the top of a glass. For the current-voltage characteristics of positive carrier only devices, a configuration of Aluminium (Al), regio-regular P3HT, poly(3,4-ethylenedioxythiophene) poly(styrenesulfonate) (PEDOT:PSS), indium tin oxide (ITO) is used. The first step is to cut ITO (150 nm) coated glass to have a size of  $1 \text{ cm}^2$ . The ITO was etched in the area of the Al contacts (left picture of Figure 11). Therefore the rest of the device was protected before etching by uniform nail polish layer (commercial product) to form a solid and thin protective layer. Etching was done using HCl:H<sub>2</sub>O ratio of 2:1. The next step is to clean the glass. The cleaning process was done in an ultrasonic bath in acetone for 10 min followed by ultrasonic bath in isopropanol and distilled water for 10 min. Next, PEDOT:PSS (100 nm) was deposited by spin-coating at 2000 rpm for 30 s and vacuum annealed at  $100^\circ \text{C}$  during 10 min. After this step, RR-P3HT (100 nm) was deposited by spin-coating at 2000 rpm for 1 min from a 7 mg/mL solution dissolved in toluene and vacuum annealed at  $100^\circ \text{C}$  during 10 min (middle picture of Figure 11). Finally, Al (150 nm) was evaporated at a base pressure of  $10^{-5}$  torr (right picture of Figure 11).

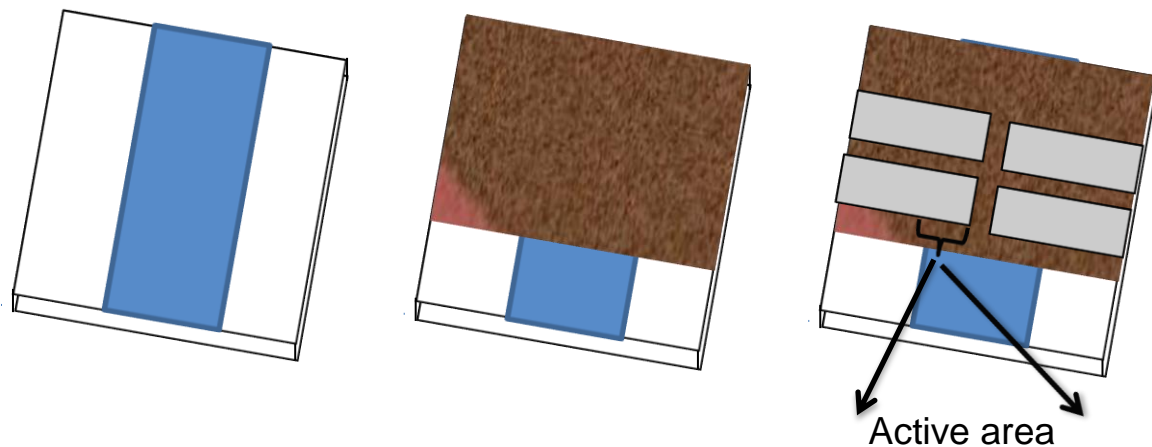


Figure 11: Left picture shows ITO glass substrate with etched ITO from the sides, middle picture shows the mixture of spin-coated solutions of P3HT and PEDOT:PSS on top of ITO, right picture shows the evaporated Al electrodes with as active area of  $0.3\text{ cm}^2$ .

To evaluate the mobility of negative charge carriers a structure of Al/CsO/P3HT/CsO/Al was used. In this work, after cleaning the glass, firstly, Al and caesium carbonate ( $\text{Cs}_2\text{CO}_3$ ) were evaporated at a base pressure of  $10^{-5}$  torr. Evaporation of  $\text{Cs}_2\text{CO}_3$  tends to deposit as a caesium oxide (CsO) layer [34]. The CsO layer of 3 nm was deposited on top of the Al. Secondly, RR-P3HT (100 nm) was spin coated with the procedure explained previously. Finally, Al and CsO were deposited again by thermal sublimation on top of RR-P3HT. Al and CsO layers thicknesses were monitored with the help of a quartz oscillator. P3HT and PEDOT:PSS thicknesses layers were measured using DektaXT surface profiler. Both RR-P3HT and  $\text{Cs}_2\text{CO}_3$  were purchased from Sigma-Aldrich. In all the devices, the active area was defined to be  $0.3\text{ cm}^2$  by using a shadow mask.

## 10. Principle of operation

Figure 12 shows the energy scheme of a positive charge carrier only device. As suggested before, to evaluate the carrier mobility using SCLC method two requirements must be fulfilled: (a) Quasi-Ohmic contact at the metal-semiconductor interface and (b) Unipolar charge injection. To satisfying both the conditions, a PEDOT:PSS layer deposited on top of ITO is chosen. PEDOT:PSS is chosen as a transport material for positive charge carrier's transport and is also known to give smooth and non-oxidizing interfaces [35]. PEDOT:PSS with a work-function of 5.2 eV [36] tends to form an Ohmic contact for efficient hole injection in RR-P3HT, which has a LUMO and HOMO energy levels of 3.0 eV and 5.0 eV, respectively [37, 38]. ITO with a work function of  $\sim 4.9$  eV [39] is needed since it is easier to contact with external wires as compared to PEDOT:PSS from our experimental point of view. The opposite lying contact Al with a work-function of 4.3 eV [40] is chosen to form injection-limited contact/barriers for the injection of both positive and negative charge carriers in P3HT, respectively. These barriers are formed due to the position of the Fermi-level of Al with respect to LUMO (HOMO) of P3HT. With ITO as positive biased, positive charge carriers (holes) can be easily injected from PEDOT:PSS to HOMO of P3HT while Al as negatively biased cannot inject negative charge carriers (electrons) due to the high energy barrier,  $\Phi_b$ , between its Fermi level and LUMO of P3HT.

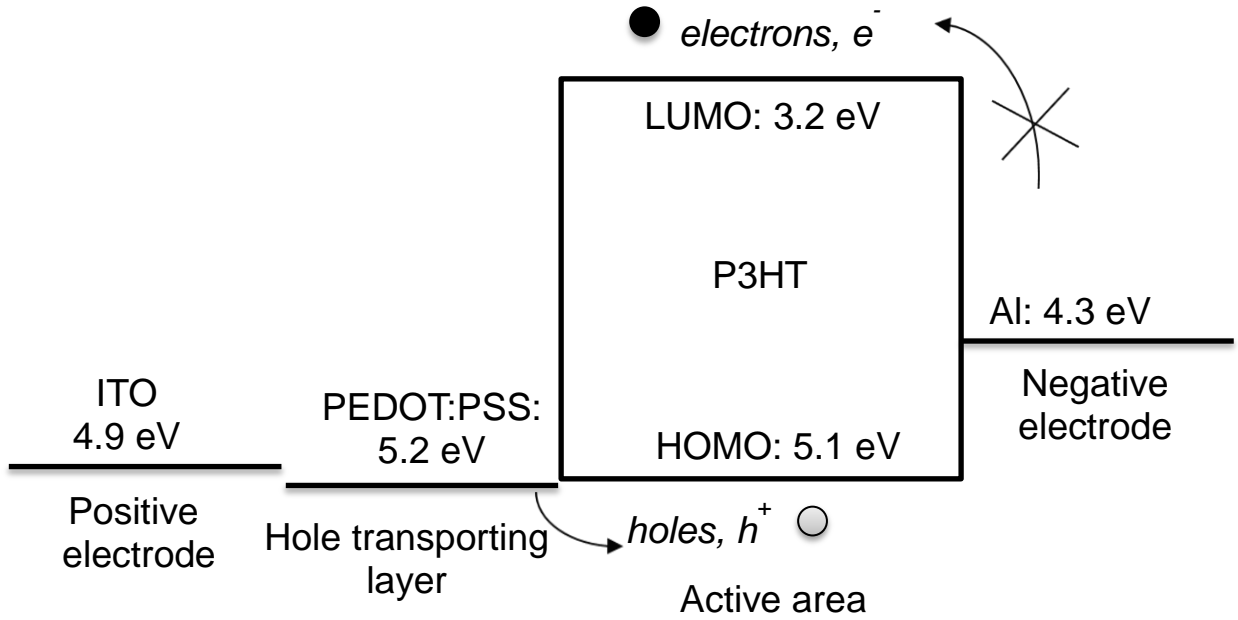


Figure 12: Schematic energy diagrams with respect to vacuum level for ITO (150 nm), PEDOT:PSS (100 nm), region-regular P3HT (100 nm), Al (150 nm), a hole-only single-carrier devices. Holes are collected via PEDOT:PSS of work-function  $\approx 5.2$  eV, by positively biased ITO electrode with work-function  $\approx 4.9$  eV. On the other hand, negatively biased Al with a work-function  $\approx 4.3$  eV cannot inject electrons due to high energy barrier between its Fermi-level and LUMO of P3HT.

Figure 13 shows the energy scheme of a negative only charge carrier device. The preparation of efficient contacts for negative charge carrier injection is more problematic, since low work function metals are highly reactive when exposed to oxygen and humidity. Recently, however, an efficient negative charge carrier injection in Alq<sub>3</sub>, Tris-(8-hydroxyquinoline) aluminium, was found by using a combination of Al/CsO [41]. Thermally evaporated CsO behaves as a heavily n-doped semiconductor exhibiting high conductivity with an intrinsically low work function. We use this strategy in our devices to inject negative charge carriers in the LUMO of RR-P3HT (Figure 13). With one of the Al/CsO electrodes as negatively biased, electrons can be easily injected to LUMO of P3HT while opposite lying Al/CsO electrode as positively



biased, cannot inject holes to HOMO of P3HT due to the due to the high energy barrier,  $\Phi_b$ , between its Fermi level and HOMO of P3HT.

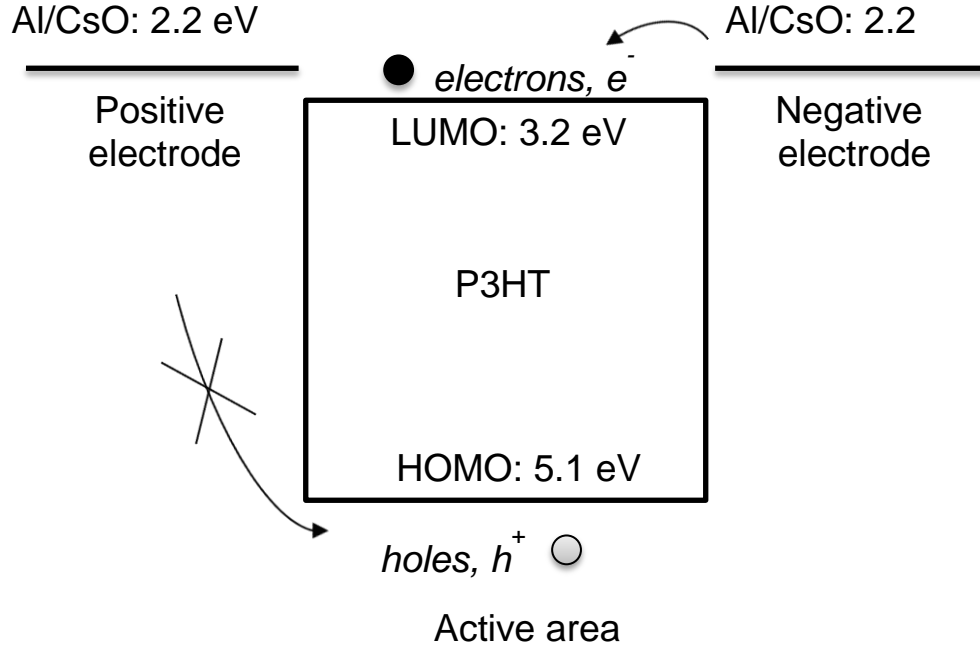


Figure 13: Schematic energy diagrams for Al (150 nm), CsO (5 nm), region-regular P3HT (100 nm), CSO (5 nm), Al (150 nm), an electron-only single-carrier device.

## 11. Results and Discussions

Current-voltage characteristics of the devices were measured using a Keithley 2602 source-meter in air. The inset plot of Figure 14 shows the log current-voltage characteristics of Al/P3HT/PEDOT:PSS/ITO diode with Al biased and PEDOT:PSS/ITO as grounded, as a hole only device. With Al(+)/P3HT/PEDOT:PSS/ITO(-), respectively the diode current attains order of magnitude in the range of mA at 3 V. On the other hand, with Al(-)/P3HT/PEDOT:PSS/ITO(+), respectively the diode current attains order of magnitude in the range of nA at 3 V. The rectification ratio, which is the ratio of currents measured at the same absolute bias, at 3 V exceeds value of  $10^6$ . This suggests that the

insertion of the PEDOT:PSS layer provides sufficient injection of positive charge carriers in P3HT. Whereas, Al forms an injection-limited contact for the injection of both positive and negative charge carriers in P3HT.

Further analysis of current-voltage characteristics of Al(+)/P3HT/PEDOT:PSS/ITO(-) diode is done by plotting its characteristics in the log current-log voltage scale (main plot of Figure 14).

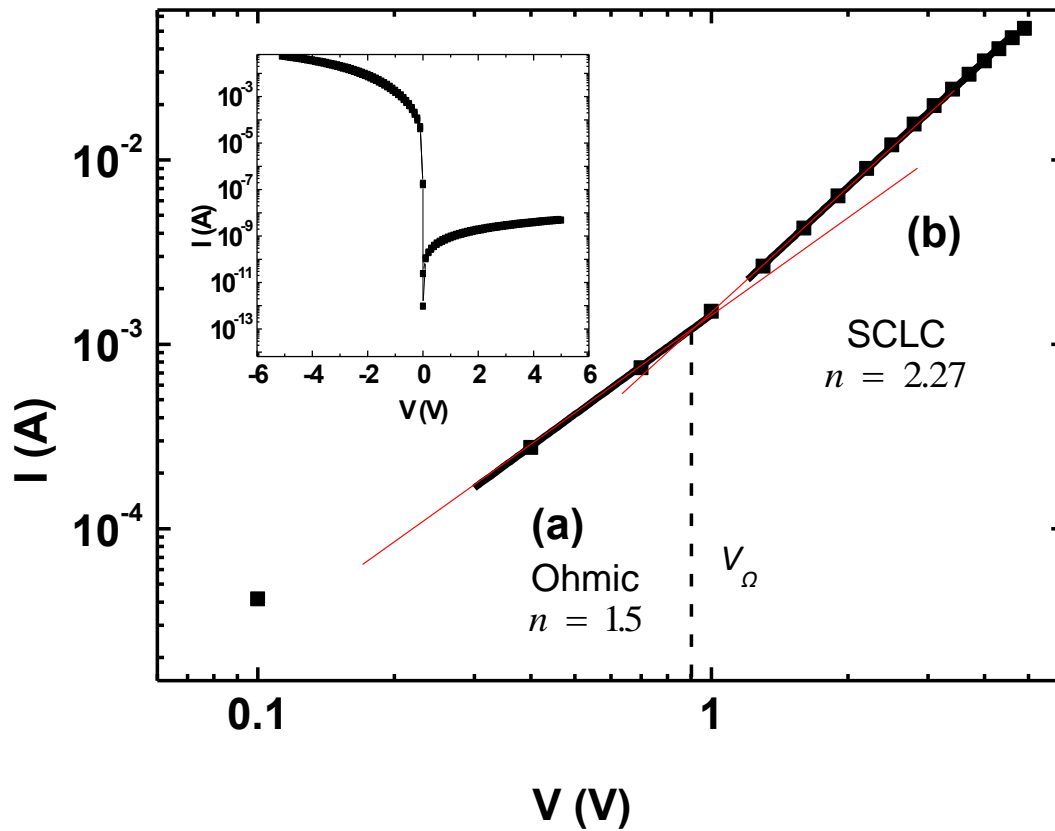


Figure 14: Inset figure shows the current-voltage characteristics of Al/P3HT/PEDOT:PSS/ITO diode with Al biased and PEDOT:PSS/ITO as grounded. Main figure shows the log-log plot of the inset figure with top contact Al/CsO negatively biased and bottom contact Al/CsO positively biased, respectively. At low voltages ( $V < 1$  V), an Ohmic region is observed and at higher voltages ( $V > 1$  V), SCLC region is observed.

---

### Evaluation of transport properties in RR-P3HT

---

It shows two distinct regions: At low voltage ( $V < 1$  V), there is an Ohmic transport region ( $I \propto V$ ) and at higher voltage ( $V > 1$  V), SCLC region occurs corresponding to  $I \propto V^2$ .

Substituting the values of  $V_Q = 0.9$  V (from the main graph),  $q = 1.6 \times 10^{-19}$  C,  $d$  (P3HT) = 100 nm,  $\epsilon_0 = 8.854 \times 10^{-12}$  Fm<sup>-1</sup>,  $\epsilon_r$  (P3HT) = 3 [42] in the equation (2-15),  $V_Q = 8/9(qp_0d^2/\epsilon)$ , one obtains the value of  $p_0 = 1.68 \times 10^{16}$  cm<sup>-3</sup>. The value of  $p_0$  represents the amount of thermally generated holes carriers in RR-P3HT at room temperature. Next step is to calculate the Ohmic and SCLC hole mobilities, respectively. Ohmic mobility can be calculated from (2-11),  $J = qp_0\mu_h V/d$ , which gives a value of  $\mu_h$  (Ohmic) =  $1.16 \times 10^{-4}$  cm<sup>2</sup>/Vs and for SCLC region the hole mobility can be calculated using (2-21),  $J = 9\epsilon\mu V^2/8d^3$ , which gives a value of  $\mu_h$  (SCLC) =  $1.35 \times 10^{-4}$  cm<sup>2</sup>/Vs.

The inset plot of Figure 15 shows the current-voltage characteristics of Al/CsO(top)/P3HT/Al/CsO(bottom) sandwich structure with top Al/CsO biased and bottom Al/CsO grounded. It can be seen that the current-voltage characteristics is almost symmetric. It means that the combination of Al/CsO on top of RR-P3HT has almost the same effect in both the cases (i) when it is deposited over P3HT and (ii) when P3HT is deposited over it, despite the fact that a native Al oxide layer is expected to be present before P3HT deposition on the bottom electrode. The obtained rectification ratio at 3 V here is  $\sim 1$ . The main plot of Figure 15 shows the log current-log voltage characteristics of Al/CsO(-)/P3HT/Al/CsO(+), respectively.

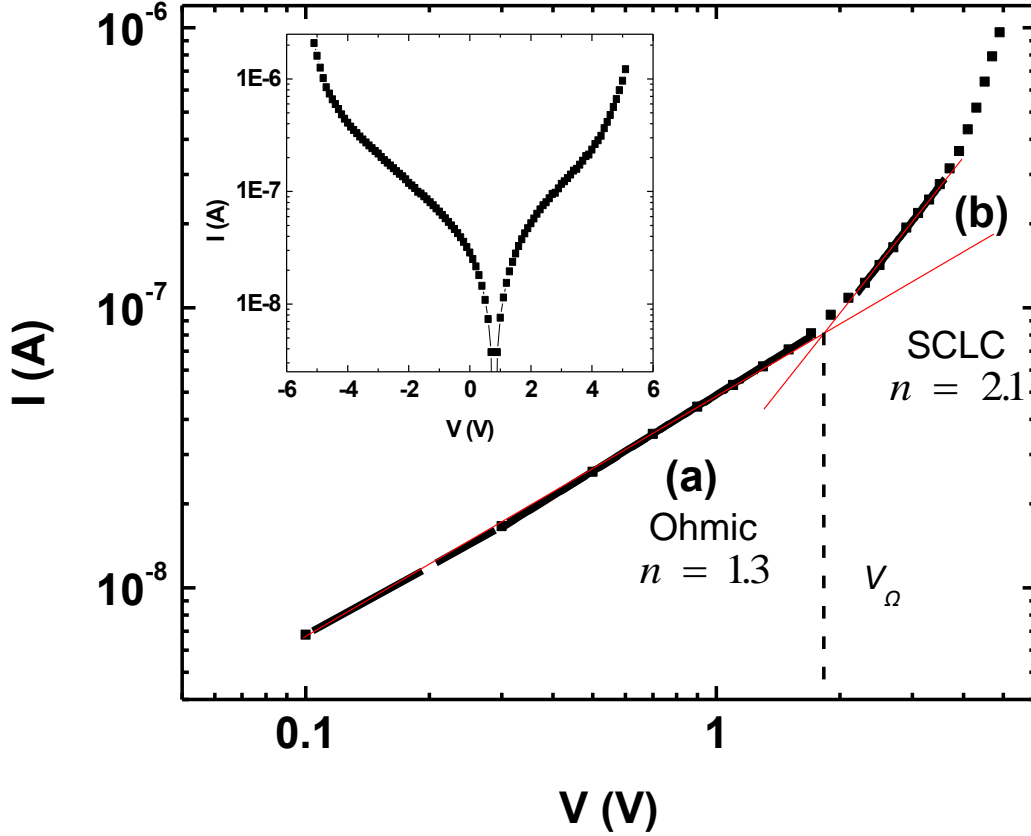


Figure 15: Inset figure shows the current-voltage characteristics of Al/CsO (top)/P3HT/CsO/Al (bottom) diode with top Al/CsO biased. Main figure shows the log-log plot of the inset figure with top contact Al/CsO negatively biased and bottom contact Al/CsO positively biased, respectively. At low voltages ( $V < 1$  V), an Ohmic region is observed and at higher voltages ( $V > 1$  V), SCLC region is observed.

Similarly to the previous results, the current-voltage characteristics of main plot show two regions: At low voltage ( $V < 1$  V), there is an Ohmic transport region ( $I \propto V$ ). At higher voltage ( $V > 1$  V), SCLC region occurs corresponding to  $I \propto V^2$ . Substituting the values of  $V_{\Omega} = 1.8$  V (from the main graph), in the equation (2-15),  $V_{\Omega} = 8/9(qn_0d^2/\epsilon)$ , one gets the value of  $n_0 = 3.36 \times 10^{16} \text{ cm}^{-3}$ . The value of  $n_0$  represents the amount of thermally generated negative carriers

---

### Evaluation of transport properties in RR-P3HT

---

in RR-P3HT at room temperature. It is important to note that the value of  $n_0$  is of the same order of magnitude of  $p_0$ . Using (2-11),  $J = qn_0\mu_h V/d$ , the obtained value of  $\mu_e$  (Ohmic) =  $1.71 \times 10^{-9} \text{ cm}^2/\text{Vs}$  and using (2-21),  $J = 9q\mu V^2/8d^3$ , the obtained value of  $\mu_e$  (SCLC) =  $1.93 \times 10^{-9} \text{ cm}^2/\text{Vs}$ , respectively.

Table 2 compares the values of the mobility obtained here with the values measured by TOF and SCLC methods in the literature. The values for positive charge carriers determined here are in good agreement with those reported in literature [32, 33, 43, 44]. However, we have found a substantially lower mobility of the negative charge carriers compared to the values obtained using TOF method. In the article that used TOF method, they claimed to use a high purity and chemical/structural regularity RR-P3HT. Also, they claimed that this is the first time such a balanced and high positive and negative charge carriers mobilities are obtained for a conjugated polymer. Although, the atmosphere in which the measurements were made is not identified. Here, the thermally generated charge carriers concentration for both holes and electrons were of the same order of magnitude, i.e.  $p_0 = n_0 = 10^{16} \text{ cm}^{-3}$ , at room temperature. It means although the thermally generated charge carrier concentrations in both carriers are of the same order of magnitude, but based on mobility values the transport of positive charge carriers is much more efficient than the negative charge carriers in RR-P3HT. The transport of negative charge carriers in RR-P3HT could be hindered due to the combination of several factors including charge transfer complex formed between RR-P3HT and oxygen due to the exposure of RR-P3HT during the fabrication and electrical characterization process. This complex is known to remove the negative charge carrier from P3HT, resulting in p-doping of P3HT [30]. Furthermore, oxygen could induce degradation of P3HT and increase trap densities resulting in lower mobilities [31].

## 12. Conclusions

An interesting conclusion can be made based on the obtained results is that when RR-P3HT is exposed to oxygen and water moieties presence, the mobility of negative charge carriers is affected decreasing by four orders of magnitude, but interestingly, the positive charge carrier's mobility remains almost unaffected. To our knowledge, this is the first time SCLC method has been used to evaluate the negative charge carrier mobility in RR-P3HT.

	<b>Methods</b>		
<b>Mobilities</b> ( $\text{cm}^2/\text{Vs}$ )	<b>TOF [32]</b>	<b>SCLC [33]</b>	<b>SCLC (this work)</b>
$\mu_h$	$3 \times 10^{-4}$	$10^{-5} - 10^{-4}$	$1.35 \times 10^{-4}$
$\mu_e$	$1.5 \times 10^{-4}$	–	$1.93 \times 10^{-9}$

Table 2: Compares obtained values of the positive ( $\mu_h$ ) and negative ( $\mu_e$ ) charge carrier mobilities using SCLC method with the mobilities values obtained using time-of-flight (TOF) method.

## 13. Future work

To verify whether the variation of the space-charge limited current follows a  $d^{-3}$  law over the thickness range of RR-P3HT, according to current density in the SCLC region  $J = 9q\mu V^2/8d^3$ . This could be done by varying the spinning speed to deposit RR-P3HT. This scaling states that for a given mean electric field, the current density decreases inversely proportional to the third power of the layer thickness of the organic semiconductor layer.

## 4. Controlled-Overflow-Transistor (COT)

---

### 1. Introduction

Today, we are living in the world of electronics and hence they immensely affect our daily life. One of the main building block of all electronic components is the transistor. During the last 60 years, electronic industry was dominated by inorganic semiconductors such as Silicon (Si) and Germanium (Ge). Despite its popularity, for some applications such as low cost, large area and flexible electronics the use of inorganic semiconductors is not an ideal choice. This led to the extensive research on various materials to find an appropriate alternative semiconductor for such applications. Organic-based electronics provided this alternative due to its promising advantages such as low-cost, simplification of production process, etc. To overcome the low mobility of organic semiconductors, the application of organic transistors requiring high output currents might be realized by the use of vertical devices. Here, charge carriers move through the device perpendicularly to the substrate and thus have to travel less than a micron.

Many inorganic transistors exhibits a vertical geometry, therefore several attempts have been made to transfer their structure to organic electronics. The modulation of current between two separated electrodes by the use of a third electrode placed in between was first reported in 1926 when E. Lilienfeld patented the vacuum tube [45]. After more than 20 years, the bipolar transistor was invented in Bell Laboratories [46], the vertical concept was applied successfully in semiconductor technology.

This chapter firstly gives a short overview of some of the transistors based on vertical architecture. It is followed by the main motivation behind the idea of Controlled-Overflow-Transistor (COT). Next, materials, fabrication process, principle of operation and

---

results obtained will be explained. Finally, conclusions based on the results COT will be analyzed and a glance at future work will be given.

## 2. Transistors based on semiconducting materials

### Metal-base transistor (MBT)

In 1932, Julius E. Lilienfeld applied for a patent on the amplification for a patent on the amplification of current in a semiconductor-metal-semiconductor structure (Figure 16) [47].

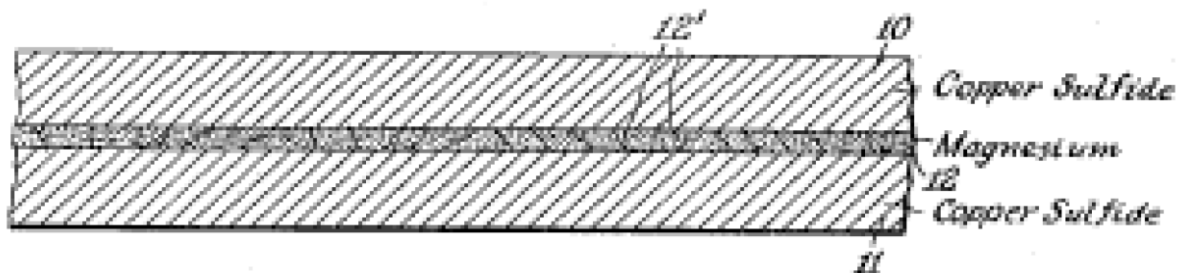


Figure 16: Lilienfeld's schematic drawing of the first current amplifier, (10), (11) marking the semiconductors and (12) a metal layer [47].

The metal-base transistor (MBT) consists of two identically doped semiconductors layers (emitter and collector) sandwiching a metal layer (base). The MBT is defined as hot-carrier device since the electrons cross the middle electrode by ballistic transport. Thermalization, which is an obvious limiting factor of the electron transfer through the base, depends upon the ratio of the base layer thickness and the mean free path for electrons in the metal. Apart from crossing the base metal, the electrons also have to overcome both emitter-base and base-collector interfaces.

---



---

### Controlled-Overflow-Transistor

---

The semiconductor materials are chosen in such a way that the energy barrier between emitter and base ( $q\phi_{BE}$ ) is higher than the energy barrier between base and collector ( $q\phi_{BC}$ ) to have efficient injection of charge carriers from emitter to collector (Figure 17) [48].

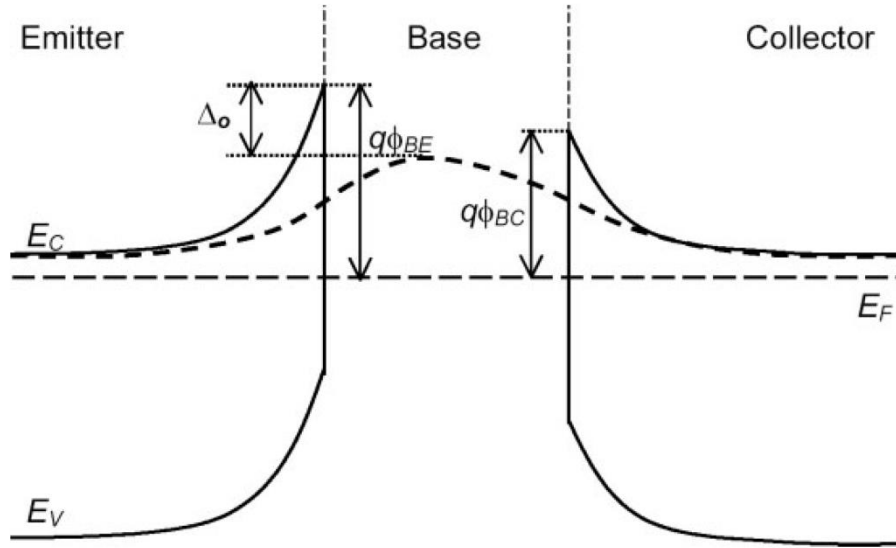


Figure 17: Energy band diagram of a MBT [48].

The current enhancement factor for common-emitter mode,  $\beta$ , is given by [21]

$$\beta = I_c/I_b \quad (4-1)$$

Thus,  $\beta$  gives the ratio of amplified output current at the collector ( $I_c$ ) to the base current ( $I_b$ ). The calculation is done similarly for common-base mode, here the common-base mode enhancement factor  $\alpha$  is obtained as the ratio of collector and emitter current:

$$\alpha = I_c/I_e \quad (4-2)$$


---

In 2004, Hümmelgen et al. reported a n-type MBT using  $C_{60}$  and n type Si (n-Si) as emitter and collector, respectively, and gold (Au) as a metal-base layer. For an operating voltage of 5 V, the common-emitter current gain of  $100 \pm 20$  is calculated [49]. In 2008, Hümmelgen et al. reported another n-type MBT in which Au was replaced by an organic conducting polymer P-type sulfonated polyaniline (SPAN) as a metal-base layer. These devices were operated at low operating voltages of 1 V to show common-emitter current gain equal to 8 [50].

### Permeable-base transistor (PBT)

Like MBT, PBT is a majority carrier device. Electrons are transferred from emitter to collector through pinholes in the base electrode instead the ballistic process known from the MBT. The current is controlled by the barrier lowering in the pinholes. The size and distribution of holes depends upon the materials used and on production. As current through openings and hot electrons add up to the collector current, the problem of defining these two contributions arises. The evidence of pinholes is provided by the measurement of the device in common-base mode. If the base is continuous, it shields the emitter from the electric field which is generated by application of collector voltage  $V_{CB}$  and no change of emitter current  $I_e$  is observed. Thus, the following equation is valid for a MBT with a continuous base:

$$\delta I_e / \delta V_{CB} = 0 \quad (4-3)$$

For PBT, emitter current is affected by the application of collector voltage  $V_{CB}$

$$\delta I_e / \delta V_{CB} \neq 0 \quad (4-4)$$

In 2009, Hümmelgen et al. reported P-type PBT using a combination of Al/ $V_2O_5$ / 2,6-diphenyl-indenofluorene layer as the emitter, a Ca/Al/Ca multilayer as the metal base, and p-Si as collector [51]. They demonstrated a hybrid organic/inorganic PBT with a low-leakage current in common-emitter mode and a highly reproducible common-emitter current gain of  $\sim 2$

independent of base current and collector voltage. In 2006, Horng et al. reported polymer space-charge-limited transistor using a Al metal grid sandwiched between poly(3-hexylthiophene). PEDOT:PSS and Al were used as emitter and collector, respectively [52]. Even though the name of the transistor is different, but the principle of operation is similar to PBT. Here, the devices were operated at a voltage of 3 V to achieve common-emitter current gain of 506.

### 3. Motivation

The previously discussed transistors i.e. MBT, PBT and polymer space-charge-limited transistors showed promising results. However, one major drawback of these transistors is low emitter-current gain. Table 3 compares the common-emitter gain values of the previously discussed transistors. The aim of this work is to further enhance the performance of organic-based transistor in vertical architecture by using a new family of transistors called as Controlled-Overflow-Transistor (COT). The basic concept of COT is take advantage of low mobility in conducting polymers. The idea is to form a blocking barrier (Schottky barrier) between conducting organic semiconductor and an inorganic semiconductor and to use the space-charge accumulation concept in the conducting organic semiconductor to control the charge overflow through a Schottky barrier. This concept goes back to almost 50 years, in which a thin film transistor operating under SCLC transport conditions was proposed using only a blocking contact to isolate the gate electrode from the active layer. To our knowledge, this is the first time that this idea has been implemented in a device.

<b>Transistors</b>	<b>current gain</b>	<b>references</b>
<b>Metal-base transistor</b>	100 ± 20	[49]
<b>Metal-base transistor</b>	8	[50]
<b>Permeable-base transistor</b>	2	[51]
<b>Polymer space- charge- limited transistor</b>	506	[52]
<b>Controlled-overflow transistor</b>	?	

Table 3 Compares the common-emitter gain values of the metal-base, permeable-base and polymer space-charge-limited transistors.

#### 4. Self-doped sulfonated polyaniline (SPAN)

In COT, a self-doped p-type conducting polymer known as sulfonated polyaniline (SPAN) is used as an active material. The following passages focuses on motivation, principle of operation and chemical synthesis of SPAN.

##### **Polyaniline**

Polyanilines are a class of polymers where doping of the neutral form involves transfer of both electrons and protons. It exists in three well defined oxidation states: leucoemeraldine, emeraldine and pernigraniline. The leucoemeraldine base is fully reduced (all amine nitrogens) whereas the pernigraniline are fully oxidized (all imine nitrogens) and emeraldine form has an imine/amine ratio of 0.5 [53]. Beginning from insulating leucoemeraldine, electrically emeraldine

can be obtained by oxidation process. Upon further oxidation, a fully oxidized pernigraniline can be obtained (Figure 18).

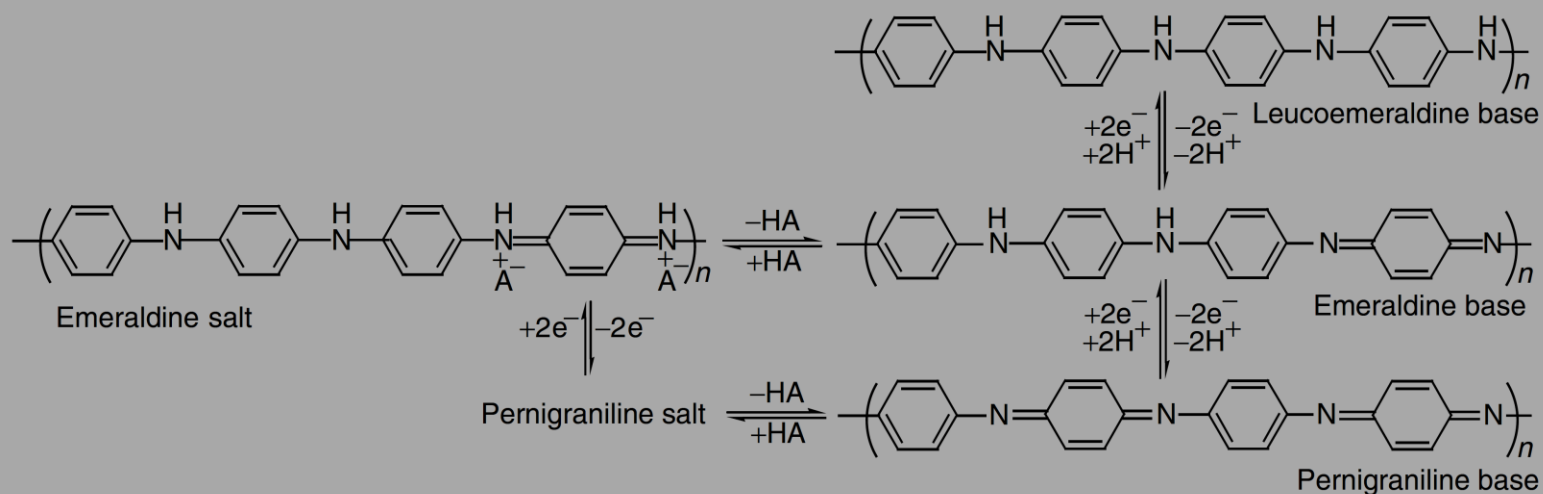


Figure 18: Different bases of polyaniline formed by oxidative and protonic doping with HA as acid proton donor.

Undoped phase amine groups ( $-NH-$ ) contains non-bonding (lone pairs) nitrogen orbitals while imine groups

( $-N=$ ) contains a mixture of lone pairs and  $\pi$ -conjugated orbitals [54].

In addition these various oxidation states can be switched between doped salt and non-doped base forms by protonation. Out of five forms of aniline, only the emeraldine salt is conducting. Polyaniline is one of the most intensively studied conducting polymers due to its unique properties such as wide range of electrical and optical tunable properties, good stability in the presence of water and humidity, high conductivity, inexpensive monomer and ease of preparation. It has been used for various applications such as transistors [55, 56], light emitting diodes [57, 58], and rechargeable batteries [59-61]. However, limitations such as poor solubility

in common solvents, pH dependent conductivity and electroactivity have limited its use in industrial applications.

### Self-doped polyaniline

To enhance the solubility of polyaniline in aqueous solution, a water soluble, self-doped, conducting polyaniline derivative known as self-doped sulfonated polyaniline was discovered in 1990 by Yue and Epstein [62] and Dao et al. [63]. Initially, polianiline in its emeraldine base form is treated with polar sulfonotric acid groups. This will result in self-doped polymer, which has the base formula of emeraldine base with sulfonated protonic groups ( $\text{SO}_3^-\text{H}^+$ ) covalently bound to its reduced and oxidized repeat groups (Figure 19)

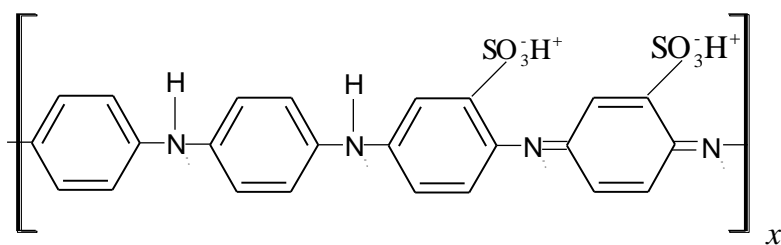


Figure 19: Semiconducting state of sulfonated polyaniline

The proton from the sulfonated group gets drawn to the imine groups, which has an immobile  $\pi$  – electron system. This will induce bipolarons on the imine group sites (Figure 20).

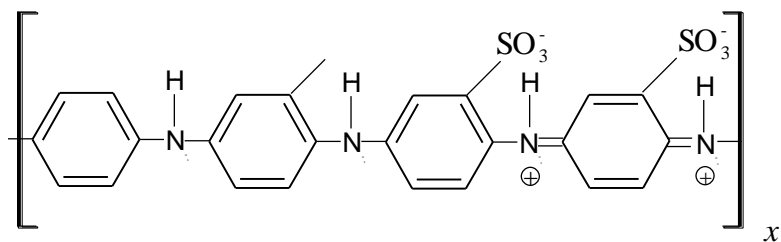


Figure 20: Formation of bipolarons

Due to internal redox reaction, bipolarons are energetically unstable and lead to the formation of two polarons with one unpaired electron per unit. The result is a half-filled and a potentially metallic state where there is a positive charge in each repeated unit with its associated counterion (Figure 21). Due to the electrostatic repulsion between the two positive charges, polarons will be separated to yield a polaron lattice [64].

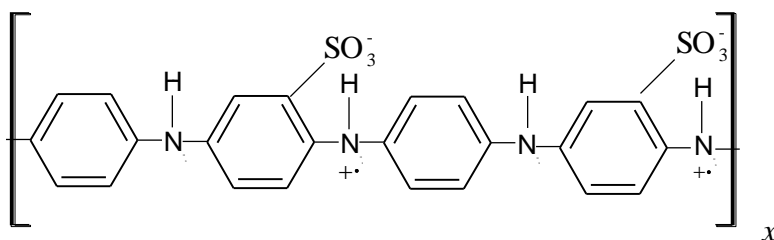


Figure 21: Conducting state of sulfonated polyaniline with no change in the number of electrons. The polarons separates, which results in a polaron lattice [64].

Figures 19-21 showed the conversion of a polyaniline emeraldine base (semiconductor) form to its emeraldine salt (conducting) form by protonation. The removal of protons will result in the polar sulfonated groups ( $\text{SO}_3^-$ ) with negative charges. The hydrophilic interactions between the sulfonated groups and polar molecules of water enhance its solubility. Thus, the sulfonate group not only improves water solubility but also acts as a charge balancing counterion when the polymer is oxidized/reduced.

The conductivity of the SPAN depends upon the degree of sulfonation and the position and nature of the side lateral group. Table 4 summarizes some of the results obtained by different research groups. Even though the solubility of polyaniline is increased by the presence of sulfonated groups along the polymer backbone, it also resulted in lowering of the conductivity. The decrease in conductivity could be attributed to twisting of the phenyl rings relative to one another and increased interchain separation (separation between two chains) due to increasing sulfonate groups density causing lowering of  $\pi$ -orbital overlap [65].

## Controlled-Overflow-Transistor

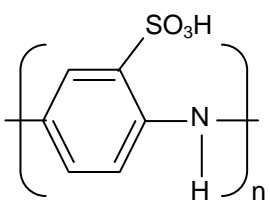
Structure	Degree of Sulfonation (%)	Conductivity (S/cm)	References
	50	0.1	[66]
	75	1.0	[67]
	100	$10^{-2}$ - $10^{-3}$	[68]

Table 4: The dependence of SPAN conductivity on the sulfonation degree.

Unlike polyaniline, sulfonated polyaniline has much stronger temperature dependence of the conductivity due to greater electron localization [68, 69, 70]. Unlike polyaniline, its conductivity is independent of pH due to the presence of intrinsic acid on the polymer backbone. The pH independence of conductivity up to 9 was reported [69].

### SPAN preparation by chemical polymerization

In this research work, SPAN is prepared by copolymerization of monomers metanilic acid (aminobenzenesulfonic acid containing sulfonic groups) and aniline with ammonium peroxodisulfate as the oxidant. The extent of doping can be tuned through the choice of metanilic acid/aniline ratios to vary the sulfonation degree by keeping the oxidant at a constant value. The method used here is similar to the method used by Yang et al. [70].



The SPAN preparation was made by using two different solutions:

- 1) 0.245 g of metanilic acid was dissolved in 400 mL of deionized water, ultrasonicated for 10 min, followed by mixing 65  $\mu$ L of aniline. The obtained solution was maintained at a constant temperature ( $\approx 10^0$  C) for one hour to stabilize aniline and to obtain homogenous films;
- 2) Ammonium persulfate was used as an oxidant to form emeraldine base form of polyaniline (Figure 18). A constant value of 2.85 g of  $(\text{NH}_4)_2\text{S}_2\text{O}_8$  dissolved in 62 mL of deionized water was used throughout the experiments. The obtained solution was kept with the previous solution at a constant temperature ( $\approx 10^0$  C) for one hour;

After one hour, the two solutions were mixed together to form SPAN. In time, the solution color changes from a transparent color (semiconducting emeraldine base form) to blue color (conducting emeraldine salt form). The whole process can be repeated to obtain different degree of sulfonation by using different concentrations of metanilic acid with respect to aniline.

SPAN can be deposited on top of different materials provided that the interaction between the surface of the material and the SPAN leads to deposition of homogeneous SPAN film on top of the material. In this work, the SPAN, which was prepared using three times the concentration of metanilic acid with respect to aniline ( $3 \times 0.245 \text{ g} : 65 \mu\text{L}$ ), was deposited on top of <100> plane surface of n-Si with a doping level of  $10^{-15} \text{ cm}^{-3}$  (Figure 22). n-Si was cleaned in a 1:1 of sulfuric and nitric acids ( $\text{H}_2\text{SO}_4:\text{H}_2\text{NO}_3$ ) bath, followed by a 10 min ultrasonic bath in distilled water. In the sequence, the samples were bathed in acetone, isopropanol and

distilled water. Finally, the silicon oxide was removed immersing the sample during 20 s in a 1:10 HF:H<sub>2</sub>O bath, where HF stands for hydrofluoric acid.

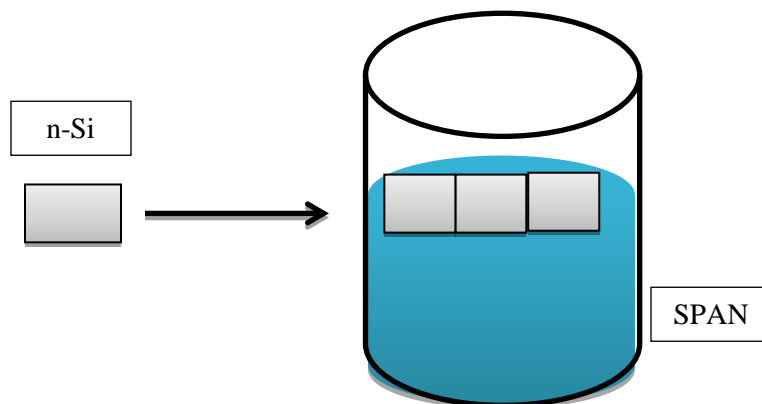


Figure 22: Schematic representation of deposition of SPAN on top of n-Si.

### SPAN thickness

To calculate the thickness of a SPAN film, a surface profilometer was used. Initially, SPAN was deposited on top of n-Si. Samples were removed at regular intervals from the beaker and the amount of time n-Si was in contact with the SPAN solution was recorded. The average thickness was measured by profilometer and was plotted with respect to the recorded time (Figure 23).

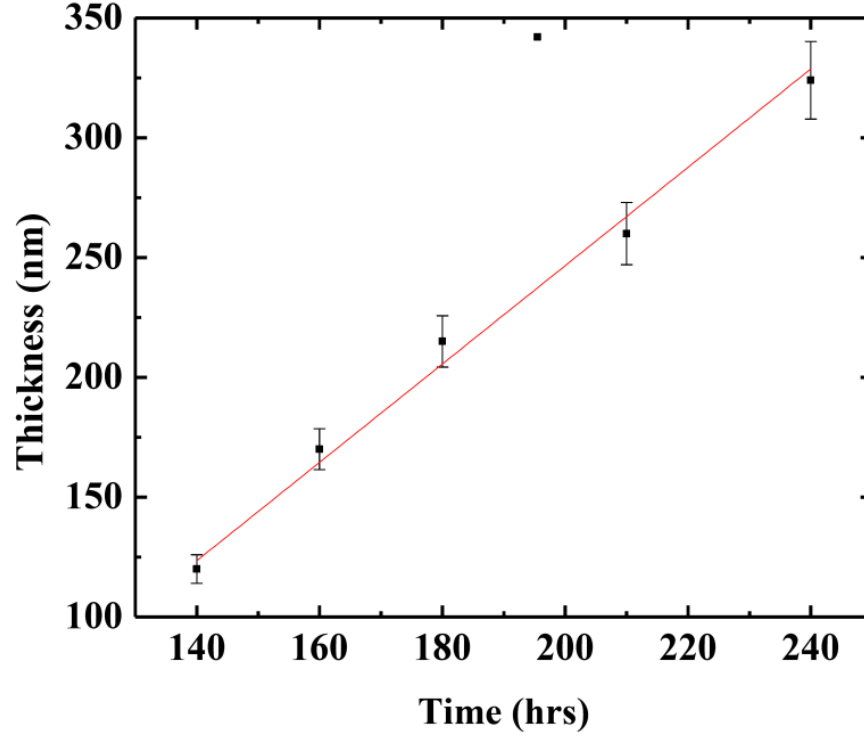


Figure 23: SPAN thickness as a function of the amount of time (in hours) n-Si was in contact in the SPAN solution.

### SPAN roughness

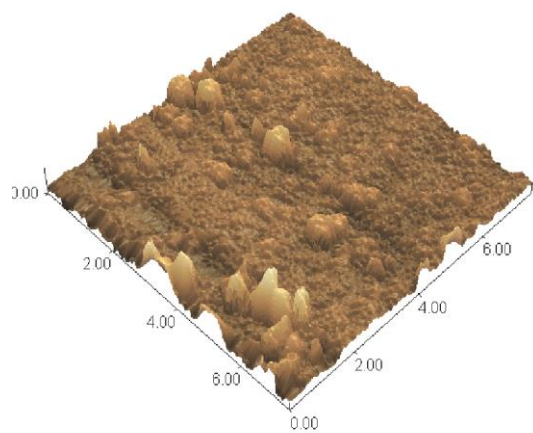
It was observed that the SPAN film layer is amorphous and the growth rate as well as its average roughness ( $R_a$ ) increases with increase in concentration of metanillic acid. This phenomenon was observed by using AFM images of the SPAN layer. The samples were prepared using the following concentrations:

## Controlled-Overflow-Transistor

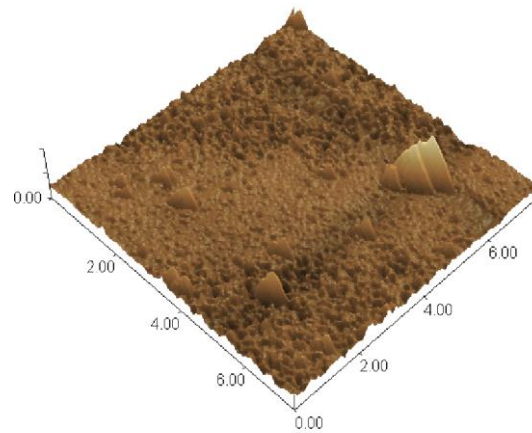
---

- 1:1 ratio of metanillic acid and aniline;
- 3:1 ratio of metanillic acid and aniline;
- 5:1 ratio of metanillic acid and aniline;
- 7:1 ratio of metanillic acid and aniline

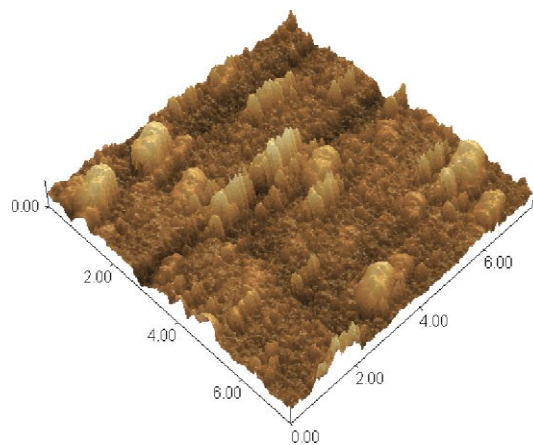
After preparation with different concentrations, samples of n-Si were removed from the SPAN solution on the third day to make a consistent comparison. AFM images showed the increase of  $R_a \approx 19$  nm for 1:1 ratio to  $R_a \approx 42$  nm for 7:1 ratio (Figure 24). Even though, the difference of  $R_a$  is very small after 3 days, but with time the difference could be large enough to make an impact on the deposition process of SPAN on top of various materials. Thickness dependence of surface morphology and its influence on the charge carrier mobility in organic semiconductor has been studied briefly before in [71].



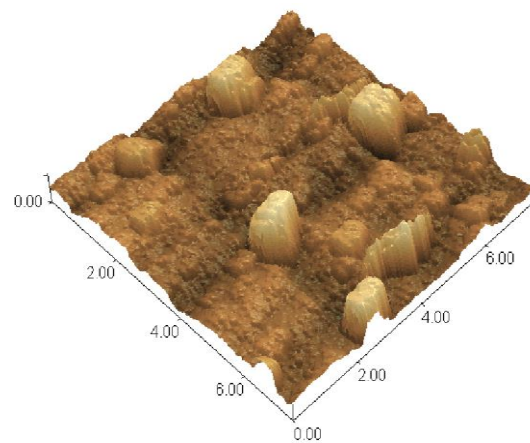
(A) 1:1 ( $R_a \approx 19$  nm)



(B) 3:1 ( $R_a \approx 20$  nm)



(C) 5:1 ( $R_a \approx 24$  nm)



(D) 7:1 ( $R_a \approx 42$  nm)

Figure 24: AFM 2D images of  $8 \times 8$  nm<sup>2</sup> SPAN prepared using (A) 1:1 (B) 3:1 (C) 5:1 (D) 7:1 concentrations of metanillic acid and aniline. The images were using the dynamic mode.

### SPAN sheet resistance

SPAN sheet resistance was performed using four-point probe method by depositing SPAN on top of a glass (Figure 25). The probe configuration used here is the linear four point probe array. In this method, two probes carry the current and other two probes measure the voltage by using a high impedance voltmeter. Since the high impedance draws very little current the effects introduced by probe resistance, probe contact resistance and spreading resistance is negligible. The voltmeter reading is equal to the voltage drop across the SPAN sheet. The sheet resistance  $R_s$  can be calculated by

$$R_s \propto V/I \quad (4.5)$$

where  $V$  is the voltage reading from voltmeter and  $I$  is the current carried by two-current carrying probes. The calculated sheet resistance of SPAN was found to be in the range of.1-6  $M\Omega/\square$  . For more detailed information on sheet resistance refer to chapter 4 of [72].

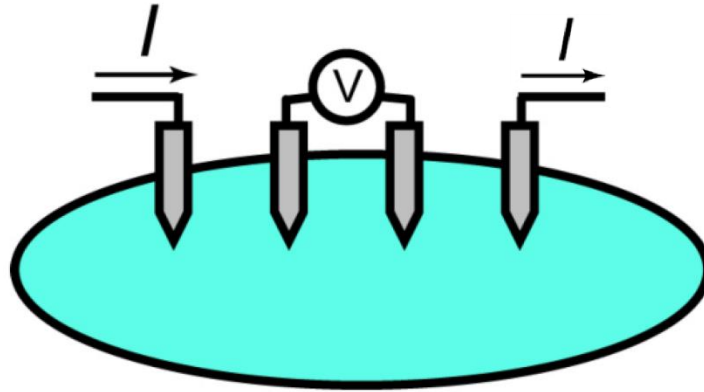


Figure 25: Schematic figure of a linear four-point probe technique used to measure SPAN sheet resistance on top of a glass.

How can a conducting polymer have such a high sheet resistance? To understand this one has to look beyond Ohm's law. It is entirely possible that the charge carrier paths in the SPAN film are hindered due to the presence of impurity and defect scattering. Usually, scattering of carrier decreases their mean-free path, which ultimately could lead to high  $R_s$ . Additionally, as discussed previously, the presence of substituents can also decrease the overlap of  $\pi$ -orbital which reduces the delocalization of  $\pi$ -electrons. The reasons mentioned are very crude as at this point there is no clear explanation for the high sheet resistance of SPAN.

To conclude, SPAN has the following properties:

- It is a p-type conducting polymer;
- Its conductivity as well as its roughness depends upon the degree of sulfonation used in preparing SPAN.
- It has a high sheet resistance;

## 5. COT fabrication

To begin with, a  $10^{15} \text{ cm}^{-3}$  phosphorus doped n-type <100> n-Si is used as a substrate. It was cleaned using sulfuric and nitric acids (50:50), acetone and isopropanol were used to remove the metallic and organic containments. After each bath, the substrate was rinsed in distilled water. The oxide layer (insulating layer) present on top of the substrate was removed by dipping it into a solution of 48 % hydrofluoric acid (HF) acid diluted in distilled water (1:10) for 20 seconds. The absence of oxide layer makes the surface of the substrate hydrophobic.

The next step is to deposit SPAN with thickness  $t$  by chemical polymerization on top of the substrate. A 3:1 ratio of metanillic acid and aniline was used in this work. The n-Si substrates were removed from the SPAN solution once it attained a desired thickness according to the previously obtained recorded time. After drying the films, Al contacts (150 nm) were evaporated as source (S) and control (CT) terminals at a base pressure of  $5 \times 10^{-6}$  torr. This process was monitored using quartz oscillator. The two contacts were separated by a channel length  $L$ . In this configuration, the channel length  $L$  is kept always larger than the SPAN thickness  $t$ . Finally, a Al:Ga eutectic alloy was applied on the Si backside to provide an ohmic contact (interconnected materials have low resistivity) acting as drain (D), see Figure 26 [73].

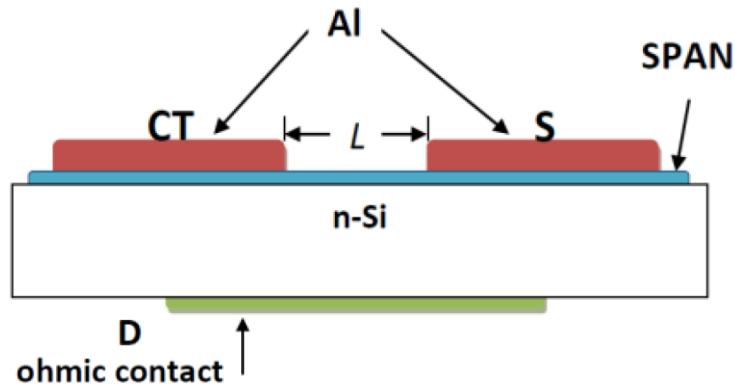


Figure 26: Schematic representation of a controlled-channel-overflow transistor using Al contacts as source and control-terminals and drain as n- Si [73].

It is important to note that both source and control terminals are made from the same material and their role is determined by the electric potential applied to the terminals. As a result, if desired, the roles of source and control-terminals can be interchanged. Compared to the vertical organic field-effect transistors (VOFETs), the structure of this device is much simpler since it does not involve an insulating layer. The elimination of this layer might reduce the production cost, time and also remove the risk of high leakage current through the insulator, which is



encountered in VOFET. Despite the absence of the insulator, the structure of this transistor is similar to an OFET, though the principle of operation is completely different.

## 6. Junction characteristics

As discussed previously, to have a breeding ground for space-charge transport in a conducting polymer, it is essential to have an ohmic or quasi-ohmic contact between the injecting metal electrode and the semiconductor. Therefore, it is important to begin by studying the density of states of SPAN. An analysis using density functional theory (DFT) simulation of an isolated molecule of SPAN at the B3LYP/3-21G(d) level of theory was done in [73]. It was found that the LUMO and HOMO of SPAN tetramer are around 3.7 eV and 5.12 eV, respectively. *Note that even though these values are obtained for SPAN tetramer, but we will apply these values of HOMO and LUMO to the SPAN film.* The obtained value of the HOMO value of SPAN matches the value obtained previously with the ionization potential of SPAN [74]. In the latter case, the HOMO value of SPAN was estimated by the Schottky energy barrier at the SPAN/n-Si interface, which by using Richardson-Schottky equation was found to be  $\approx 1.0$  eV to the silicon electron affinity ( $\approx 4.1$  eV) [23]. It was also found by using DFT simulation that the density of states has a group of four unoccupied electronic states very close to 3.65 eV, see Figure 27 [73]. These unoccupied states can be filled by the electron injection from a low work function metal.

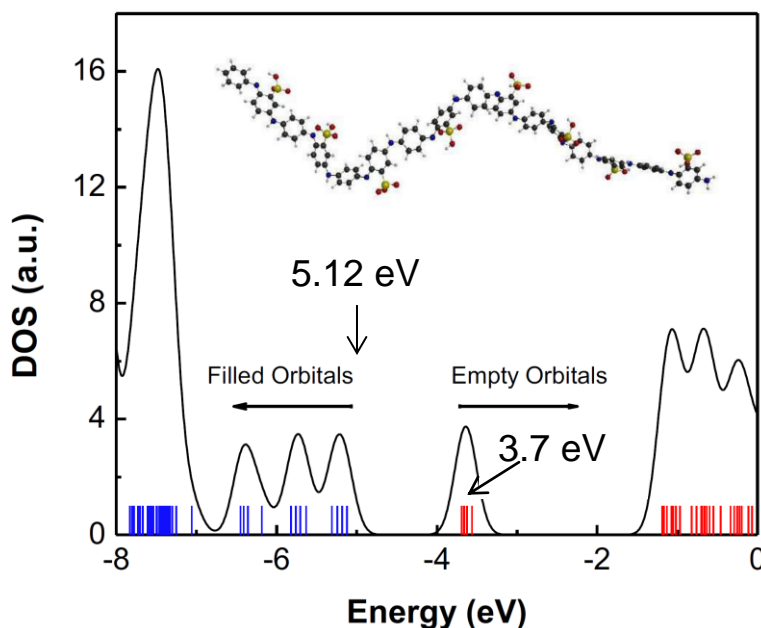


Figure 27: Density of electronic states of SPAN tetramer as a function of the energy with respect to the vacuum level. The average position of LUMO is at 3.7 eV below the vacuum level. HOMO is approximately at 5.12 eV. Inset: ground state geometry of the SPAN tetramer [73].

We used Al and Au with work-functions of 4.3 eV and 5.1 eV [40, 75] to verify the presence of the low energy tail of the empty states distribution in the SPAN. To confirm the above assumption practically, we used a diode structure of Al(-)/SPAN/n-Si/Al(+) and Au(-)/SPAN/n-Si/Al(+) devices. Using the current-voltage characteristics, the idea behind these devices is to fabricate an electron-only device and observe which metal electrode is able to better transport electrons giving higher currents in SPAN. Figure 28 compares the current-voltage characteristics of both devices [73]. It is clear that the current values in the case of Al are much higher than the Au. These results confirm that LUMO energy levels of SPAN are located around the work function of Al. Ohmic injection at the SPAN/ Al interface was reported in [76]. However, in the latter case, SPAN was prepared by electrochemical polymerization instead of chemical polymerization. *It is important to note that the electrons of Al, when injected into the SPAN, will become minority carriers since SPAN is a p-type conducting polymer.* All the devices were

electrically characterized in the air and in the dark using an Agilent 4155C semiconductor parameter analyzer.

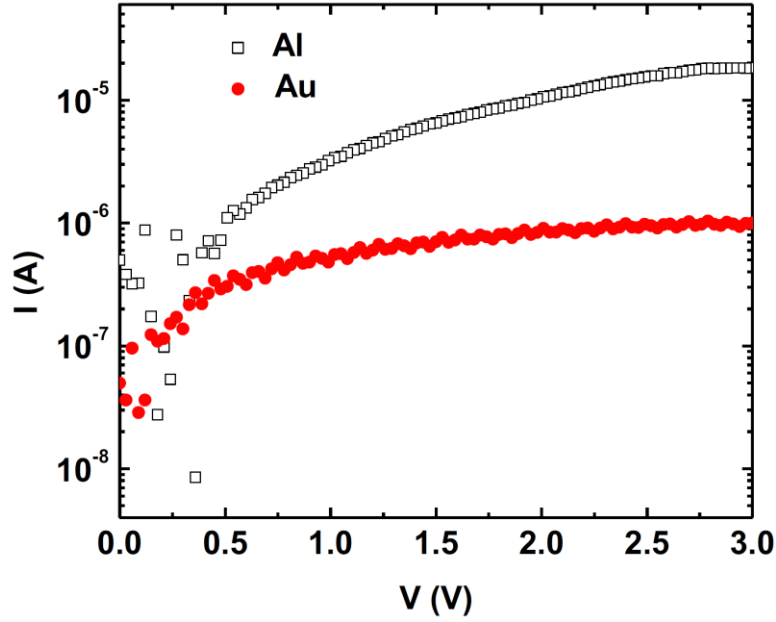


Figure 28: Electron only current of Al(-)/SPAN/n-Si/Al(+) and Au(-)/SPAN(+)/n-Si/Al(+) devices obtained in the air and dark [73].

## 7. Results and Discussions

### Principle of operation

To have a better understanding of all the peculiarities of the device operation, a simple model of two parallel diodes is used here. After explaining this model, it will be compared to the measured current-voltage characteristics of the device. In this way, it will be simple to understand the mechanisms of the transport of charge carriers in the device.

---

### Controlled-Overflow-Transistor

---

This device can be pictured as a parallel association of two reverse biased Schottky junctions between (1) control-terminal and drain terminals (CT-D) and (2) source and drain terminals (S-D). These two junctions are separated by the resistance of the SPAN layer (Figure 29). The current along the SPAN film between S and CT is  $I_{S \rightarrow CT}$ , the current between CT and D diode is  $I_{CT \rightarrow D}$  and the current between S and D diode is  $I_{S \rightarrow D}$ .

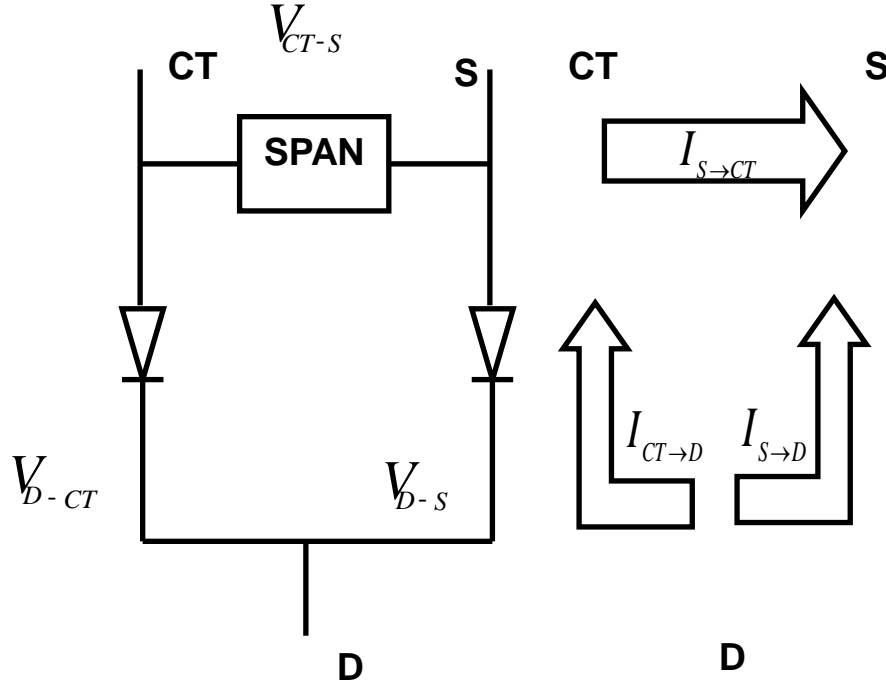


Figure 29: Schematic representation of a model with two parallel Schottky diodes between CT-D and S-D with its respective currents.

Initially, when there is no electrical potential applied between the control-terminal and the source terminals ( $V_{CT-S} = 0 \text{ V}$ ), it is expected that the currents  $I_{CT \rightarrow D} \approx I_{S \rightarrow D} = 0$ , since the contacts have the same area and therefore as a result  $I_D = I_{CT \rightarrow D} + I_{S \rightarrow D} \approx 2 I_{S \rightarrow D} = 0$ . If we consider two diode junctions (S-D and CT-D) as independent and non-interacting, then the application

---

---

## Controlled-Overflow-Transistor

---

of  $V_{CT-S}$  should reduce the potential difference between terminals D and CT ( $V_D - V_{CT}$ ). As a consequence, the current  $I_{CT \rightarrow D}$  also decreases. Since  $I_D = I_{CT \rightarrow D} + I_{S \rightarrow D}$ , decrease in  $I_{CT \rightarrow D}$  also reduces the total current  $I_D$ . After establishing this understanding, the same principle of operation can be compared with the transistor characteristics of the devices.

Using the common-source output configuration, a configuration in which source terminal as negatively biased (grounded) is common to positively biased control and drain terminals, see Figure 30. The applied electrical potential difference between drain and source terminals is given by  $V_{D-S}$ .

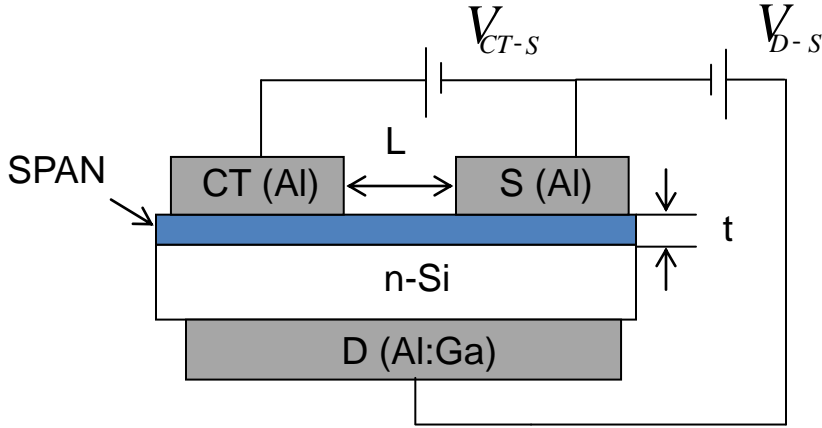


Figure 30: Schematic representation of the COT in the common-source configuration.

Figure 31 represents the  $I_D(V_{D-S})$  output characteristics of the COT in the common-source mode. The first curve (black) shows the current  $I_D$  at drain without the application of  $V_{CT-S}$ . It can be seen that the current  $I_D$  between source and drain terminals increases with increasing

---

$V_{D-S}$ , when  $V_{CT-S} = 0$  V. Next, with the application of  $V_{CT-S} = 0.1$  V, the current  $I_D$  (red) not only increases with increasing  $V_{D-S}$ , but is also modulated by  $V_{CT-S}$ . The current on-off ratio, which defines how efficient the current  $I_D$  can be modulated by the application of  $V_{CT-S}$ , at 5 V is  $I_D(V_{CT-S} = 0.1 \text{ V})/I_D(V_{CT-S} = 0 \text{ V}) \approx 1$ . Ideally, a high current on-off ratio is desired for fast switching time of the device. Here, the low current on-off ratio is due to the high output current  $I_D$  when  $V_{CT-S} = 0$  V. Therefore, the current  $I_D(V_{CT-S} = 0 \text{ V})$  is called as the leakage current. The lower the current  $I_D(V_{CT-S} = 0 \text{ V})$ , the higher will be the current on-off ratio and the faster the device can switch from off-to-on state. The problem of this high leakage current could be attributed to the energy location of the SPAN LUMO with respect to the silicon electron affinity. Electrons injected from the Al into the SPAN are at higher energies and the barrier present at SPAN/n-Si interface is not high enough to create an obstacle for these electrons. With the further increase in  $V_{CT-S}$ , the output current  $I_D$  modulates further.

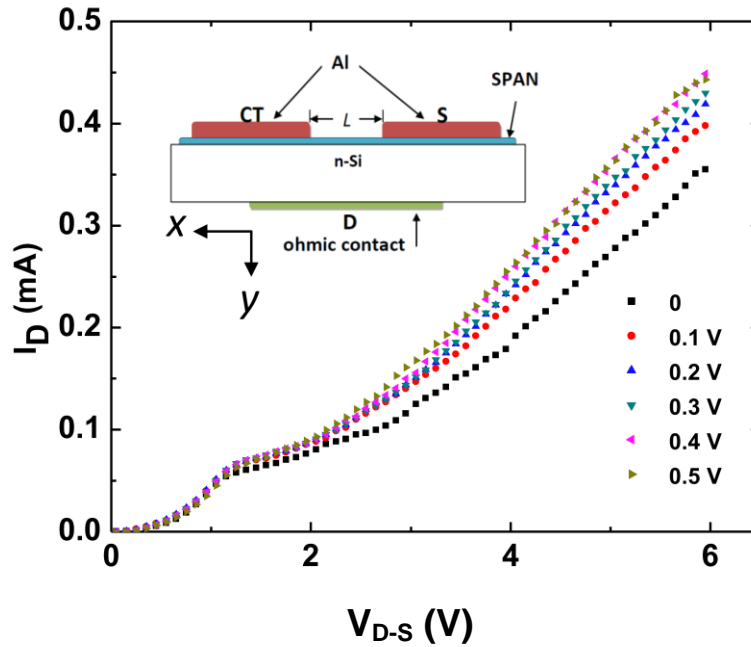


Figure 31: Characteristic curves  $I_D(V_{D-S})$  of the device ( $L = 45 \mu\text{m}$  and  $t = 200 \text{ nm}$ ) for different  $V_{CT-S}$  ranging from 0 to 0.5 V. Inset: Device structure with the corresponding axes taken from [73].

Figure 32 shows the schematic energy diagram of COT. The principle of operation of COT can be understood as follows: when  $V_{CT-S}$  is applied, electrons from the source (Al) are injected into the unoccupied electronic states of SPAN. Due to the high sheet resistance and low mobility (discussed later) of SPAN film, charges will accumulate near the injecting contact. With small thickness of the SPAN layer and due to electrostatic repulsion between the injected charge carriers, electrons tends to spread along the SPAN layer in the direction perpendicular to the Al/SPAN interface. Since the SPAN layer thickness  $t$  is smaller than the channel length  $L$ , the amount of negative charges accumulated can fill the unoccupied electronic states and can be high enough for the electrons to acquire a sufficient potential energy to overcome the Schottky energy barrier at SPAN/n-Si interface. The electric field present at the Schottky barrier will then drift the charge carriers to n-Si. It is important to note that charges get accumulated at both sides (1) near the Al/SPAN injecting contact (due to low mobility of the conducting material) and (2) at SPAN/n-Si interface (due to the presence of blocking contact).

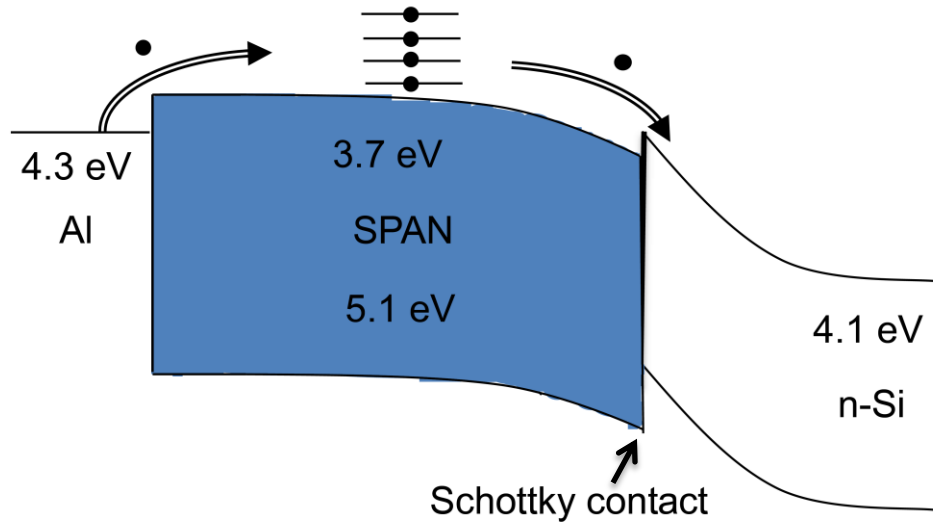


Figure 32: Schematic energy diagram of COT.

Contrary to the diode model, it is clear that the current  $I_D$  increases with  $V_{CT-S}$ . There must be some additional effect which is increasing the current  $I_{S \rightarrow D}$  larger than the reduction of  $I_{CT \rightarrow D}$ . Under these circumstances, both diodes show different current-voltage characteristics. The gain comes from the fact that the current along the SPAN layer between source and control-terminals  $I_{S \rightarrow CT}$  is small, due to the high sheet resistance of SPAN, than the  $I_{S \rightarrow D}$  so that  $(I_{CT \rightarrow D} + I_{S \rightarrow D})/I_{S \rightarrow CT} > 1$ . This common-source current gain ( $\beta$ ) can be defined by the relationship:

$$\beta = (dI_D / dI_{CT}) \quad (4.6)$$

To understand the physics behind the increase of  $I_{S \rightarrow D}$  under the application of a positive  $V_{CT-S}$ , current-voltage characteristics in Figure 30 will be characterized into two regimes namely SCLC and thermionic based on lower and higher electric field strengths.

### **SCLC regime**

With the observation of a quasi-Ohmic contact at Al/SPAN interface, charge carries are injected upon the application of  $V_{D-S}$  and accumulated near the injecting contact. This charge accumulation gives rise to SCLC phenomenon along the SPAN layer, which further limits the charge carrier transport between Al electrodes and n-Si. Figure 33 shows the current-voltage characteristics in the log-log scale with the angular coefficient of 2 (dark line). For  $V_{CT-S} < V_{D-S} < 1$ , the current  $I_D$  has a power-law dependence on  $V_{D-S}$  and almost does not depend on  $V_{CT-S}$ . The  $I_D \times V_{D-S}$  characteristics in this regime can be described by Mott-

---



Gurney's law and mobility can be calculated by using the equation (2.21). Using the value of SPAN thickness of  $t = 200$  nm and fitting to the experimental data, the calculated mobility value of electrons in the SPAN is  $\mu = 2.2 \times 10^{-7} \text{ cm}^2 \text{ V}^{-1} \text{ S}^{-1}$ . This results show that not only SPAN has high sheet resistance but also has low electron mobility. Note that in this voltage range,  $I_D$  drops with increase in  $V_{CT-S}$  for a fixed  $V_{D-S}$ . This is due to the fact that  $I_{CT \rightarrow D}$  decreases with increasing  $V_{CT-S}$ , while  $I_{S \rightarrow D}$  remains constant.

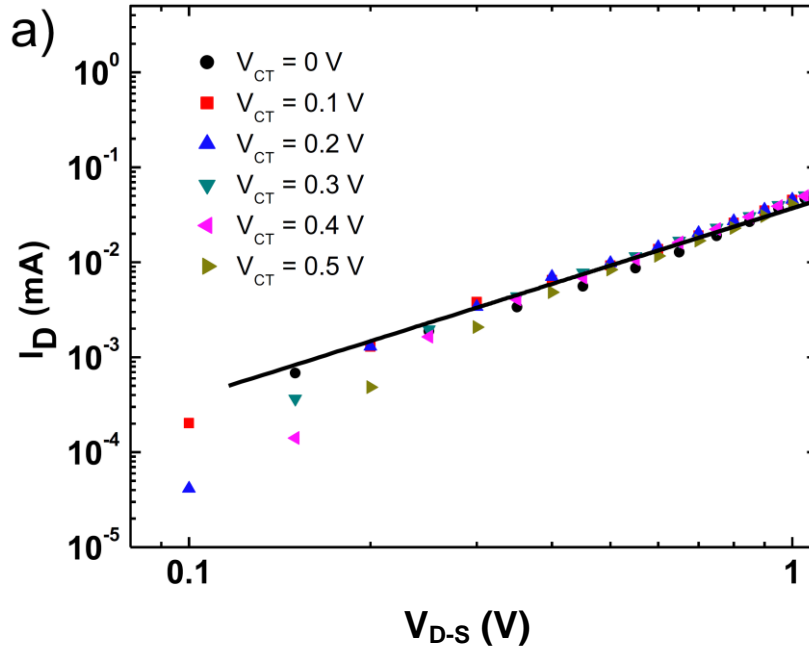


Figure 33: log-log plot of the  $I_D(V_D)$  data of Figure 30 for different  $V_{CT-S}$  in the range  $V_D < 1$  V. The continuous line is a power-law fit to the experimental data with exponent 2 [73].

### Thermionic regime

With increase in  $V_D$ , the quasi-Fermi level for electrons at the blocking contact of SPAN/n-Si interface rises due to charge accumulation so that the effective barrier height at Schottky diode is

lowered due to the Schottky effect. As a result, a significant density of electrons can overcome the blocking contact and reach the silicon layer. This will drain the accumulation of carrier at the Al/SPAN interface. Thus, the  $I_D \times V_D$  characteristics reach a new regime where the current flow is limited by the thermionic injection over the reduced barrier at SPAN/n-Si interface.

We performed an analysis of  $I_D$  dependence on  $V_{CT-S}$  in the range of  $V_{D-S} > 1$  V to demonstrate the presence of Schottky effect and the reason behind the increase of  $I_{S \rightarrow D}$  upon the application of  $V_{CT-S}$ . Figure 33 shows the  $\ln[I_D] \times V_D^{1/2}$  (main plot) of the experimental data of Figure 30 for  $V_{CT-S} = 0$  V and 0.5 V. Starting with analyzing the measured curves without the application of  $V_{CT-S}$  (open circles). The linear curve fits the experimental data with an angular coefficient of 1.53. This value was compared to the theoretically calculated value of angular coefficient by using (2-7)  $\Delta\phi_B = [q\xi/4\pi\epsilon_s]^{1/2}$  where  $\epsilon_s$  is the electrical permittivity of n-Si. In the thermionic regime, one can write  $I_D \approx I_{S \rightarrow D} + I_{CT \rightarrow D} = I_0 \left( \exp\left[\sqrt{q\xi_{CT \rightarrow D}/4\pi\epsilon_s}\right] + \exp\left[\sqrt{q\xi_{S \rightarrow D}/4\pi\epsilon_s}\right] \right)$  where  $\xi_{CT \rightarrow D}$  and  $\xi_{S \rightarrow D}$  are the electric fields in the n-Si at S-D and CT-D diodes, respectively. These fields are related to the respective fields in the polymer layer by the ratio between SPAN and n-Si dielectric constants or

$$\xi_{S \rightarrow D} = (\epsilon_{pol}/\epsilon_s) \xi_{s \rightarrow d}^{pol} \text{ and } \xi_{CT \rightarrow D} = (\epsilon_{pol}/\epsilon_s) \xi_{CT \rightarrow D}^{pol} \quad (4.7)$$

$I_0$  is the drain current at the transition between SCLC regime and thermionic regime each crossing Schottky junction. If  $V_{CT-S} = 0$  V, the electric field at the S-D and CT-D diodes is equal. Assuming  $\xi_{CT \rightarrow D}^{pol} = \xi_{S \rightarrow D}^{pol} = V_{D-S}/t$  and using (4-7), we find that  $I_{D0} = 2I_0 \exp[\alpha_t V_D^{1/2}]$  when  $V_{CT-S} = 0$  V, where coefficient  $\alpha_t$  is given by

$$\alpha_t = \sqrt{q\epsilon_{pol}/4\pi(\epsilon_s KT)^2} \quad (4.8)$$

Taking  $t = 200 \text{ nm}$ ,  $\epsilon_{pol} = 3\epsilon_0$ ,  $\epsilon_s = 3.8\epsilon_0$  and  $T = 300 \text{ K}$  in (4-8), one gets  $\alpha_t = 1.606$ . This small difference between the values of the angular coefficient obtained by the fitting in Figure 34 and the value calculated using (4.8) might be due to fact local electric field at the SPAN/n-Si interface is different than the average value of electric field, estimated while calculating, along the SPAN layer. This result suggested that the Schottky effect is the mechanism behind increase of  $I_D$  with  $V_{D-S}$ . The above theoretically calculated value of angular coefficient was performed by Koehler et al. [73].

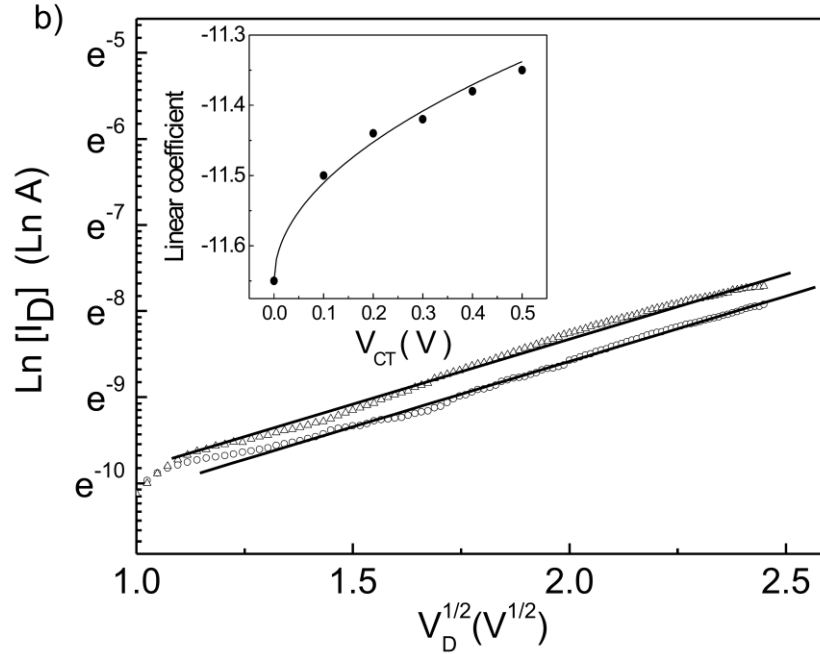


Figure 34:  $\ln I$  versus  $V^{1/2}$  plot of Figure 42 for  $V_{CT-S} = 0 \text{ V}$  and  $0.5 \text{ V}$  in the range  $V_{D-S} > 1 \text{ V}$ . The continuous lines are straight lines fitting to the experimental data. Inset: The linear coefficient of the continuous lines in the  $\ln I$  versus  $V^{1/2}$  plot [73].

Figure 34 shows the dependence of  $I_D$  with the application of  $V_{CT-S}$ . One can see that curve with  $V_{CT-S} = 0.5 \text{ V}$  is a straight line parallel to the line measured with  $V_{CT-S} = 0 \text{ V}$  in the

---

### Controlled-Overflow-Transistor

---

$\ln [I_D] \times V_{D-S}^{1/2}$  plot. Similarly the curves for other values of  $V_{CT-S}$  (0.1, 0.2, 0.3, and 0.4 V) measured formed a family of straight lines parallel to the line obtained with  $V_{CT-S} = 0$  V (those curves are not shown in Figure 33 to preserve the plot's clarity). The inset to Figure 33 shows the linear coefficients of the straight lines (with angular coefficient equals to 1.53) that fit the experimental data for different  $V_{CT-S}$  in the  $\ln [I_D] \times V_{D-S}^{1/2}$  plot. The results in Figure 34 suggest that the variation of  $I_D$  upon the application of  $V_{CT-S}$  comes from an additional Schottky effect across the SPAN/Si diode due to the extra electric field created by the control voltage.

In the thermionic regime,  $V_{D-S}$  is considerably higher than  $V_{CT-S}$ . We thus model the dependence of  $I_D$  on  $V_{CT-S}$  by assuming that the current between the source and drain is enhanced by an additional component along the y-direction of the electric field ( $\xi_{CT \rightarrow S}$ ) created by the application of  $V_{CT-S}$ . Figure 35 shows the distribution of electric field lines in COT by the application of  $V_{CT-S}$  and  $V_{D-S}$ . The distribution of field lines (black) of the electric field created by  $V_{CT-S}$  is not only in the direction of CT and S electrodes (responsible for  $I_{CT-S}$ ) in the x-direction, but also connecting the metallic source to n-Si in the y-direction. This additional component of  $V_{CT-S}$  in the y-direction is the reason behind the increase of  $I_{S \rightarrow D}$  upon the application of  $V_{CT-S}$ . The electric field lines (red) created by the  $V_{D-S}$  is in y-direction.

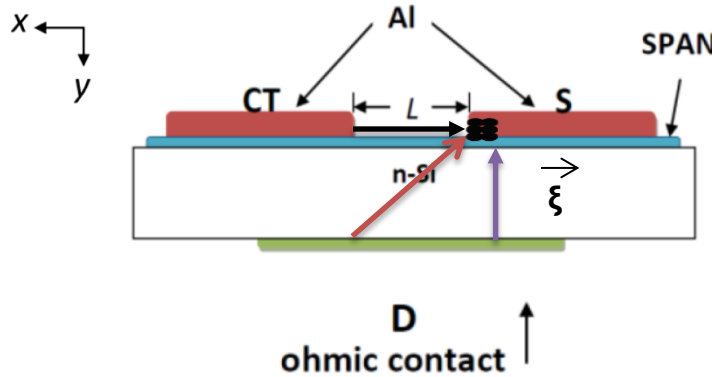


Figure 35: Schematic figure of electric field lines in the colors blue and black produced by the voltages  $V_{CT-S}$  and  $V_{D-S}$ , respectively. The additional effect in COT comes from the distribution of electric field lines produced by  $V_{CT-S}$  in x as well as y-direction.

---

## 8. Current gain

It was observed that the resistance along the SPAN layer increases with increasing  $L$  and decreasing  $t$ . This decrease in resistance can be understood from the relation,  $R = \rho(L/A)$ . If  $t$  is thin, the injected charge carriers along the SPAN layer are uniformly distributed, which could reduce the accumulation of charges at the Al/SPAN interface. As SPAN thickness grows, charge accumulation at the interface leads to SCLC followed by Schottky effect leading to higher gain. However, if  $t$  increases too much, the resistance of the SPAN film in the direction perpendicular to the SPAN/n-Si become too high. Therefore, transistor can be optimized by adjusting the ratio between SPAN thickness to length of the gap between S and CT,  $t/L$ , in order to maximize the ratio between charge density overcoming the barrier to charge flowing along the SPAN channel

Figure 36 shows the current gain plot at  $L=45\ \mu\text{m}$  and  $t=200\ \text{nm}$  at  $V_D = 5\text{V}$ . Using equation (6.1), the obtained current gain is:

$$\beta = (dI_D/dI_{CT}) = \pm 2077$$

Comparing the common-source gain values of the previously mentioned transistors in Table 3, one finds the gain obtained here is almost 4-5 times higher than others.

---

### Controlled-Overflow-Transistor

---

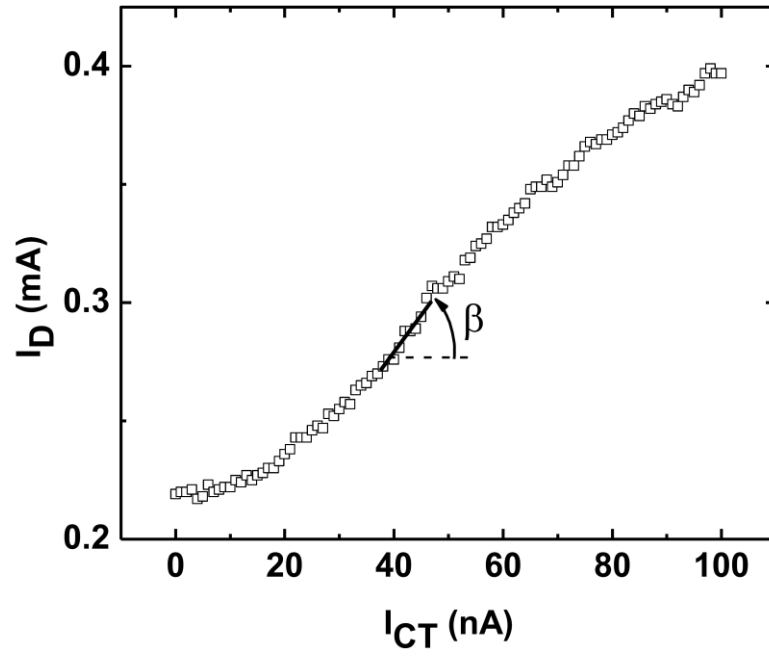


Figure 36:  $I_D(V_D)$  device characteristic for ( $L = 45 \mu m$  and  $t = 200 nm$ ) at  $V_D = 5 V$  to calculate the  $\beta = \pm 2077$  [73].

Table 5 below compares the common-emitter gain obtained with different  $L$  and  $t$  devices at  $V_D = 5 V$ . Conditions where gain was not observed are indicated by "—".

$L$ ( $\mu m$ )	$t$ (nm)			
	150	200	225	250
22	$\pm 1475$	$\pm 214$	—	—
45	—	$\pm 2077$	$\pm 1169$	—
100	—	—	—	—

Till this part, all the previously stated experiments results were published in [73]. Unfortunately, we could not further investigate the device because the aniline that was used in preparing the SPAN was finished. Newly synthesized aniline was used to repeat the experiments, but the devices could not reproduce the results.

## 9. Conclusions

### Advantages

- Low production cost and less time consuming in fabrication since the deposition of insulating layer is eliminated;
- This transistor produces a high common-source output current in the order of mA with very low operating voltage;
- Shows high current gain depending upon the thickness of SPAN and the distance between two Al electrodes. Table 6 below compares some of the current gains obtained for different architectures of transistors

Transistors	current gain	references
Metal-base transistor	$100 \pm 20$	[49]
Metal-base transistor	8	[50]
Permeable-base transistor	2	[51]
Polymer space- charge-limited transistor	506	[52]
Controlled-overflow transistor	$\pm 2077$	

Table 6: Comparisons of current gain achieved with different configurations of the transistors.

- The transistor structure used here can also be applied to other organic and inorganic materials;

### Drawbacks

- One big challenge of this device is that it suffers from a high leakage current;
- Device performance depends upon the properties the chemical nature of SPAN. This is a difficult to control since the SPAN properties depends upon many factors like the monomers used and the preparation method;

### 10.Future work

- To repeat the previous results with the application of new synthesized aniline and then to further enhance the performance of the device;
- Leakage current may be controlled by forming a thin silicon oxide or by use different combination of materials at the SPAN/n-type Si interface to form an effective injection limiting barrier;
- To test the device with magnetic-field application;



## References

---

- [1] S. Frenkel, *Plastic: A Toxic Love Story*. Houghton Mifflin Harcourt, 2011.
  - [2] H. P. Kallman, M. Pope and P. Magnanate, *Electroluminescence in Organic Crystals*, Journal of Chemical Physics, 1963. **38**(8) p. 2042-2043.
  - [3] H. Shirakawa, E. J. Louis, A. G. MacDiarmid, C.K. Chiang, and A. J. Heeger, *Synthesis of electrically conducting organic polymers – halogen derivatives of polyacetylene, (CH)<sub>x</sub>*, Journal of the Chemical Society-Chemical Communications, 1977. (16) p.578-580.
  - [4] R. W. Gundlach, *Xerography from the beginning*, Journal of Electrostatics, 1989. **24** p. 3–9.
  - [5] C. W. Tang, S. A. Vanslyke, and C. H. Chen, *Electroluminescence of doped organic thin-films*, Journal of Applied Physics, 1989. **65**(9) p. 3610–3616.
  - [6] C. J. Brabec, N. S. Sariciftci, and J. C. Hummelen, *Plastic Solar Cells*, Advanced Functional Materials, 2001. **11**(1) p. 15-26.
  - [7] Z. Bao, A. Dodabalapur, and A. J. Lovinger, *Soluble and processable regioregular poly(3-hexylthiophene) for thin film field-effect transistor applications with high mobility*, Applied Physics Letters, 1996. 69(26) p. 4108-4110.
  - [8] J. H. Burroughes, D. D. C Bradley, A. R. Brown, R. N. Marks, K. Mackay, R. H. Friend, P. L. Burns, and A. B. Holmes, *Light-emitting diodes based on Conjugated polymers*, Nature, 1990. **347**(11) p. 539-541.
  - [9] <http://orgworld.de/>
  - [10] A. J. Mozer, P. Denk, M. C. Scharber, H. Neugebauer, and N. S. Sariciftci, *Novel Regiospecific MDMO-PPV Copolymer with improved Charge Transport for Bulk Heterojunction Solar Cells*, The Journal of Physical Chemistry B, 2004. **108** p. 5235-5242.
-

## References

---

- [11] W. D. Gill, Drift mobilities in amorphous charge-transfer complexes of trinitrofluorenone and poly-n-vinylcarbazole *Journal of Applied Physics*, 1972. **43**(12) p. 5032-5040.
  - [12] H. Bässler, Charge Transport in Disordered Organic Photoconductors a Monte Carlo Simulation Study, *Physica status solidi B*, 1993. **175**(1) p. 15.
  - [13] P. M. Borsenberger, and D. S. Weiss, “*Organic Photoreceptors for Imaging Systems*” (Marcel Dekker, New York, 1993).
  - [14] F. W. Schmidlin, *Theory of trap-controlled transient photoconduction*, *Physics Review B*, 1977. **16** p. 2362-2385.
  - [15] L. Li, G. Meller, and H. Kosina, *Influence of traps on charge transport in organic semiconductors*, *Solid-State Electronics*, 2007. **51**(3) p. 445-448.
  - [16] D. C. Hoesterey, and G. M. Letson, *The trapping of photocarriers in anthracene by anthraquinone, anthrone and naphacene*, *Journal of Physics and Chemistry of Solids*, 1963. **24**(12) p. 1609-1615.
  - [17] G. Horowitz, R. Hajlaoui, D. Fichou, and A. El Kassmi, *Journal of Applied Physics*, 1999. **85**(6) p. 3202-3206.
  - [18] M. Abkowitz, and D. M. Pai, *Comparison of the drift mobility measured under transient and steady-state conditions in a prototypical hopping system*, *Philosophical Magazine Part B*, 1986. **53**(3).
  - [19] W. E. Spear, *Drift mobility techniques for the study of electrical transport properties in insulating solids*, *Journal of Non-Crystalline Solids*, 1969. **1**(3) p. 197-214.
  - [20] G. Juška, K. Genevičius, G. Sliaužys, A. Pivrikas, M. Scharber, and R. Österbacka, *Double injection current transients as a way of measuring transport in insulating organic films*, *Journal of Applied Physics*, 2007. **101** p. 114505.
-

## References

---

- [21] S. M. Sze, *Metal-Semiconductor Contacts, in Physics of Semiconductor Devices*, Singapore, 2<sup>nd</sup> Edition, 1981. **250**.
- [22] Heinz K. Henisch, *Semiconductor contacts: An approach to idea and models*, Oxford, 1984.
- [23] J. G. Simmons, *Poole-Frenkel Effect and Schottky effect in metal-Insulator-Metal Systems*, Physics Review, 1967, **155** p. 657-660.
- [24] M. A. Lampert and P. Mark, *Current injection in solids – I*, New York and London, Academic Press, 1970.
- [25] D. Ma, I. A. Hümmelgen, B. Hu and F. E. Karasz, *Electron and hole transport in a green-emitting alternating block copolymer: space-charge-limited conduction with traps*, Journal of Applied Physics, 1999. **32** p. 2568-2572.
- [26] Z. Bao, A. Dodabalapur, and A. J. Lovinger, *Solution and processable regioregular poly(3-hexylthiophene) for thin film field-effect transistor applications with high mobility*, Applied Physics Letters, 1996. **69**(26) p. 4108-4110.
- [27] M. Jefferies, and R. D. McCullough, *Regioregular Polythiophenes*, Vol. 1 (CRC press, New York, 2007).
- [28] H. Sirringhaus, P. J. Brown, R. H. Friend, M. M. Nielsen, K. Bechgaard, B. M. W. Langeveld-Voss, A. J. H. Spiering, R. A. J. Janseen, E. W. Meijer, P. Herwig, and D. M. de Leeuw, *Two-dimensional charge transport in self-organised, high-mobility conjugated polymers*, Nature, 1999. **401** p. 685-688.

## References

---

- [29] C. Goh, R. J. Kline, M. D. McGehee, E. N. Kadnikova, and J. M. J. Frechet, *Controlling the Field-Effect Mobility of Regioregular Polythiophene by Changing the Molecular Weight*, Advanced Materials, 2003. **15**(18) p. 1519-1522.
  - [30] M. S. A. Abdou, F. P. Orfino, Y. Son, and S. Holdcroft, *Interaction of Oxygen with Conjugated Polymers: Charge Transfer Complex Formation with Poly(3-alkylthiophenes)*, Journal of Americal Chemical Society, 1997. **119** p. 4518-4524.
  - [31] J. Schafferhans, A. Baumann, C. Deibel, and V. Dyakonov, *Trap distribution and the impact of oxygen-induced traps on the charge transport in poly(3-hexylthiophene)*, Applied Physics Letters, 2008. **93** p. 093303.
  - [32] S.A. Choulis, Y. Kim, J. Nelson, D. D. C. Bradley. M. Giles, M. Shkunov, and I. McCulloh, *High ambipolar and balanced carrier mobility in regioregular poly(3-hexylthiophene)*, Applied Physics Letters, 2004. **85**(17) p. 3890-3892.
  - [33] C. Goh, R. J. Kline, M. D. McGehee, E. N. Kadnikova, and J. M. J. Frechet, *Molecular-weight-dependent mobilities in regioregular poly(3-hexyl-thiophene) diodes*, Applied Physics Letters, 2005, **86** p. 122110(1-3).
  - [34] T. R. Briere, and A. H. Sommer, *Low-work-function surfaces produced by cesium carbonate decomposition*, Journal of Applied Physics, 1977. **48**(8) p. 3547-3550.
  - [35] L. B. Groenendaal, F. Jonas, D. Freitag, and H. Pielartzik, J. R. Reynolds, *Poly(3,4-ethylenedioxythiophene) and Its Derivaties: Past, Present and Future*, Advanced materials, 2000. **12**(7) p. 481-494.
  - [36] T. W. Lee, Y. Kwon, J.J. Park, L. Pu, T. Hayakawa, and M. A. Kakimoto, *Novel Hyperbranched Phthalocyanine as a Hole injection Nanolayer in Organic Light-Emitting Diodes*, Macromolecular journal.
-

## References

---

- [37] L. Micaroni, F. C. Nart, and I. A. Hümmelgen, *Considerations about the electrochemical estimation of the ionization potential of conducting polymers*, Journal of Solid State Electrochemical, 2002. **7** p. 55-59.
- [38] R. Valaski, L. M. Moreira, L. Micaroni, and I. A. Hümmelgen, *Charge injection and transport in electrochemical films of poly(3-hexylthiophene)*, Journal of Applied Physics, 2002. **92**(4) p. 2035-2040.
- [39] T. W. Lee, and Y. Chung, *Control of the Surface Composition of a Conducting –Polymer Complex Film to Tune the Work Function*, Advanced Functional Materials, 2008. **16** p. 2246-2252.
- [40] K. L. Wang, B. Lai, M. Lu, X. Zhou, L. S. Liao, M. M. Ding, X. Y. Hou, and S. T. Lee, *Electronic structure and energy level alignment of Alq<sub>3</sub>/Al<sub>2</sub>O<sub>3</sub>/Al and Alq<sub>3</sub>/Al interfaces studied by ultraviolet photoemission spectroscopy*, 2000. **363** p. 178-181.
- [41] P. Tyagi, R. Srivastava, A. kumar, S. Tuli, and M. N. Kamalasanan, *Effect of doping of cesium carbonate on electron transport in Tris(8-hydroxyquinolino) aluminium*, Organic Electronics, 2013. **14** p. 1391-1395.
- [42] G. Garcia-Belmonte, A. Munar, E. M. Barea, J. Bisquert, I. Ugarte, and R. Pacios, *Charge carrier mobility and lifetime of organic bulk heterojunctions analyzed by impedance spectroscopy*, Organic Electronics, 2008. **9** p. 847-851.
- [43] B. Huang, E. Glynos, B. Frieberg, H. Yang, P. F. Green, *Effect of thickness-dependent microstructure on the out-of-plane hole mobility in poly(3-hexylthiophene) films*, Applied Materials and Interfaces, 2012. **4** p. 5204-5210.
- [44] A. M. Ballantyne, J. S. Wilson, J. Nelson, D. D. C. Bradley, J. R. Durrant, M. Heeney, W. Duffy, I. McCulloh, *TOF mobility measurements in pristine films of P3HT: Control of hole*

## References

---

- injection and influence of film thickness*, Organic Photovoltaics VII, 2006. **6334** p. 633408 (1-11).
- [45] J. E. Lilienfeld, *Method and apparatus for controlling electric currents*, U.S. Patent No. 1, 745, 175, Filed Oct 8, 1926, Issued Jan 18, 1930.
- [46] J. Bardeen, and W. H. Brattain, *The Transistor, A semiconductor Triode*, Physical Review, 1948. **74**(2) p.230.
- [47] J. E. Lilienfeld, "Amplifier for electric currents, 1932.
- [48] M. S. Meruvia and I. A. Hümmelgen, *Hybrid Molecular/Inorganic Semiconductor Transistors in Vertical Architectures*, 2006. **16** p. 459-467.
- [49] M. S. Meruvia, I. A. Hümmelgen, M. L. Sartorelli, A. A. Pasa and W. Schwarzacher, *Organic-metal-semiconductor transistor with high gain*, Applied Physics Letters, 2004. **84**(20) p. 3978-3980.
- [50] W. J. da Silva, I. A. Hümmelgen, R. M. Mello and D. Ma, *Hybrid meal-base transistor with base of sulfonated polyaniline anf fullerene emitter*, Applied Physics Letters, 2008. **93** p. 053301 (1-3).
- [51] J. P. M. Serbena, J. YHuang, D. Ma, Z. Y. Wang and I. A. Hümmelgen, *Vertical structure permeable-base hybrid transistors based on multilayered metal base for stable electrical characteristics*, Organic Electronics, 2009. **10** p. 357-362.
- [52] Y-C Chao, H-F Meng and S-F Horng, *Polymer space-charge-limited transistor*, Applied Physics Letters, 2006. **88** p. 223510 (1-3).
-

## References

---

- [53] J. C. Chiang, and A. G. MacDiarmid, *Polyaniline - protonic acid doping of the emeraldine form to the metallic regime*, Synthetic Metals, 1986. **13**(1-3) p. 193-205.
  - [54] H. S. Nalwa, Ed., “*Handbook of Organic Conductive Molecules and Polymers*” Vols. 1-4. Wiley, New York, 1997.
  - [55] R. K. Yuan, S. C. Yang, H. Yuan, R. L. Jiang, H. Z. Qian, and D. C. Gui, *Surface field-effect of polyaniline film*, Synthetic Metals, 1991. **41** p. 727.
  - [56] K. S. Lee, G. B. Blanchet, F. Gao, and Y. L. Loo, *Direct patterning of conductive water-soluble polyaniline for thin-film organic electrodes*, Applied physics letters, 2005. **86** p. 074102(1-3).
  - [57] G. Gustafsson, Y. Cao, G. M. Treacy, F. Klavetter, N. Colaner, and A. J. Heeger, *Flexible light-emitting diodes made from soluble conducting polymers*, Nature, 1992. **357** p. 477.
  - [58] Y. Yang, E. Westerweele, C. Zhang, P. Smith, and A. J. Heeger, *Enhanced performance of polymer light-emitting diodes using high-surface area polyaniline network electrodes*, Journal of Applied physics, 1995. **77** p. 694.
  - [59] T. Sotomura, H. Uemachi, K. Takeyama, K. Naoi, and N. Oyama, *New organodisulfide polyaniline composite cathode for secondary lithium battery*, Electrochimica Acta, 1992. **37** p.1851.
  - [60] E. M. Genies, and S. Picart, *Is the use of polyaniline associated with sulfur compounds of interest for battery electrodes*, Synthetic Metals, 1995. **69** p. 165.
  - [61] N. Oyama, T. Tatsuma, T. Sato, and T. Sotomura, *Dimercaptan-polyaniline composite electrodes for lithium batteries with high-energy density*, Nature, 1995. **373** p. 598.
-

## References

---

- [62] J. Yue, A. J. Epstein, *Synthesis of self-doped conducting polyaniline*, Journal of the American Chemical Society, 1990. **112** p. 2800.
- [63] J. Y. Bergeron, J. W. Chevalier, and L. H. Dao, *Water-soluble conducting poly(aniline) polymer*, Chemical Communications, 1990. p. 180-182.
- [64] S. Stafstrom, J. L. Bredas, A. J. Epstein, H. S. Woo, D. B. Tanner, W. S. Huang, A. G. MacDiarmid, *Polaron lattice in highly conductive polyaniline: Theoretical and optical studies*, 1987. **59**(13) p. 1464-1467.
- [65] J. H. Fendler, *Self-assembled nanostructured materials*, Chemistry of materials, 1996. **8** p. 1616.
- [66] J. Yue, Z. H. Wang, K. R. Cromack, A. J. Epstein, A. G. MacDiarmid, *Effect of sulfonic acid group on polyaniline backbone*, Journal of the American Chemical Society, 1991. **113** p. 2665.
- [67] X. L. Wei, Y. Z. Wang, S. M. Long, C. Bobeczko, A. J. Epstein, *Synthesis and physical properties of highly sulfonated polyanilines*, Journal of the American Chemical Society, 1996. **118** p. 2545.
- [68] J. Yue, G. Gordon, A. J. Epstein, *Comparison of different synthetic routes for sulfonation of polyaniline*, Polymer, 1992. **33** p. 4410.
- [69] H. Q. Tng, A. Kitani, S. Ito, *Electrochemical copolymerization of aniline and aniline-2,5-disulfonic acid*, Electrochimica Acta, 1997. **42**, 3421.
- [70] C. H. Yang, L. R. Huang, Y. K. Chih, W. C. Lin, F. J. Liu, and T. L. Wang, *Molecular assembled self-doped polyaniline copolymer ultra-thin films*, Polymer, 2007. **48** p. 3237-3247.
-



## References

---

- [71] T. Xue-Yan, X. Zheng, Z. Su-Ling, Z. Fu-Jun, Y. Guang-Cai, L. Jing, S. Qin-Jun, W. Yun, and X. Xu-Rong, *Thickness dependence of surface morphology and charge carrier mobility in organic field-effect transistors*, Chinese Physical Society, 2010. **19**(1) p. 018103 (1-6).
- [72] E. Bogatin, *Signal and Power Integrity*, 2<sup>nd</sup> edition, Boston, July 2009.
- [73] M. F. Ahmed, K. F. Seidel, C. F. N. Marchiori, R. M. Q. Mello, M. Koehler, and I. A. Hümmelgen, *Hybrid vertical transistor based on controlled lateral channel overflow*, Journal of Applied Physics, 2012. **112** p. 074509(1-7).
- [74] W. J. da Silva, I. A. Hümmelgen, and R. M. Q. Mello, *Sulfonated polyaniline/n-type silicon junctions*, Journal of Mater Science, 2009. **20** p. 123-126.
- [75] D. R. Lide, *CRC Handbook of Chemistry and Physics*, CRC, Boca Raton, 1995.
- [76] R. M. Q. Mello, and I. A. Hümmelgen, *Ohmic contacts between sulfonated polyaniline and metals*, Journal of Solid State Electrochemistry, 2001. **5** p. 546-549.